This is a preprint, the final version is subject to change, of the American Mineralogist (MSA)
Cite as Authors (Year) Title. American Mineralogist, in press.
(DOI will not work until issue is live.) DOI: http://dx.doi.org/10.2138/am-2017-6004

REVISION 1

Multi-Stage formation of REE Minerals in the Palabora Carbonatite Complex, South Africa

R. Johannes Giebel[1,2], Christoph D.K. Gauert[2,3], Michael A.W. Marks[1], Gelu Costin[4,5] and Gregor Markl[1]

1) Department of Geoscience, Eberhard Karls University, Wilhelmstr. 56, 72076 Tübingen, Germany

2) Department of Geology, University of the Free State, 250 Nelson-Mandela-Drive, Bloemfontein 9300, South Africa

3) Department of Applied Geology and Geohazards, Geological Survey of Saxony-Anhalt, Köthener Str. 38, 06118 Halle (Saale), Germany

4) Department of Geology, Rhodes University, PO Box 94, Artillery Road, Grahamstown 6140, South Africa

5) Department of Earth Science, Rice University, 6100 Main Street, Houston, TX, 77005, U.S.A

Abstract

The 2060 Ma old Palabora Carbonatite Complex (PCC), South Africa, comprises diverse REE mineral assemblages formed during different stages and reflects an outstanding instance to understand the evolution of a carbonatite-related REE mineralization from orthomagmatic to late-magmatic stages and their secondary post-magmatic overprint. The ten rare earth element minerals monazite, REE-F-carbonates (bastnäsite, parisite, synchysite), ancylite, britholite, cordylite, fergusonite, REE-Ti-betafite and anzaite are texturally described and related to the

evolutionary stages of the PCC. The identification of the latter five REE minerals during this study represents their first described occurrences in the PCC as well as in a carbonatite complex in South Africa.

The variable REE mineral assemblages reflect a multi-stage origin: 1. Fergusonite and REE-Ti-betafite occur as inclusions in primary magnetite, bastnäsite is enclosed in primary calcite and dolomite. These three REE minerals are interpreted as orthomagmatic crystallization products. 2. The most common REE minerals are monazite replacing primary apatite, and britholite texturally related to the serpentinization of forsterite or the replacement of forsterite by chondrodite. Textural relationships suggest that these two REE-minerals precipitated from internally derived late-magmatic to hydrothermal fluids. Their presence seems to be locally controlled by favorable chemical conditions (e.g. presence of precursor minerals which contributed the necessary anions and/or cations for their formation). 3. Late-stage (post-magmatic) REE minerals include ancylite and cordylite replacing primary magmatic REE-Sr-carbonates, anzaite associated with the dissolution of ilmenite, and secondary REE-F-carbonates. The formation of these post-magmatic REE minerals depends on the local availability of a fluid, whose composition is at least partly controlled by the dissolution of primary minerals (e.g., REE-fluorocarbonates).

This multi-stage REE mineralization reflects the interplay of magmatic differentiation, destabilization of early magmatic minerals during subsequent evolutionary stages of the carbonatitic system and late-stage fluid-induced remobilization and re-/precipitation of precursor REE minerals. Based on our findings, the Palabora Carbonatite Complex experienced at least two successive stages of intense fluid–rock interaction.

Keywords: rare earth minerals; Loolekop; monazite, britholite, anzaite, fluoro-carbonates, ancylite, cordylite, fergusonite, REE-Ti-betafite

Introduction

Carbonatites are important exploration targets for rare earth elements (REE) and high field strength elements (HFSE, e.g., Mariano 1989; Wall and Mariano 1996; Verplanck et al. 2016). Since REE have become increasingly important for industrial use (Chakhmouradian and Wall 2012; Hatch 2012; Wall 2014) and were categorized as critical and strategic metals (European-Commission 2014; Nassar et al. 2015), the scientific interest to understand the complex REE mineralizations found in carbonatitic systems has tremendously increased (e.g., Verplanck et al. 2016). Processes potentially responsible for REE enrichment in carbonatites include fractional crystallization of carbonatitic magma, enrichment of REE in magmatic fluids and subsequent precipitation, breakdown of primary carbonatitic minerals with sequestration of REE in secondary minerals and subsolidus redistribution of REE (e.g., Verplanck et al. 2016). In all these processes, REE-bearing minerals (such as apatite, calcite, and dolomite) have to be distinguished from actual REE minerals with REE as major constituents. The most common REE minerals in carbonatites include REE-phosphates (mostly monazite) and various hydrous and anhydrous carbonates (e.g., ancylite, burbankite and carbocernaite) and fluorocarbonates, such as bastnäsite, parisite and synchysite (e.g., Wall and Zaitsev 2004b; Kanazawa and Kamitani 2006).

This study presents detailed textural observations on the various REE phases in the Loolekop pipe of the Palabora Complex (South Africa) (PCC). These textural relations to both the carbonatitic minerals and among each other are used to distinguish between orthomagmatic, late-magmatic and post-magmatic stages of formation and provide a better understanding for the importance of fluid-assisted mobilization and reprecipitation of these minerals. Understanding these typically late-stage processes is crucial for any economic judgement on REE in carbonatites (Wall and Zaitsev 2004a; Chakhmouradian and Zaitsev 2012; Zaitsev et al. 2015). Accordingly, the aim of this study is to present the crystallization and alteration

history of the various REE minerals within the different evolutionary stages observed the PCC as a prime example of REE-mineralized, large carbonatitic systems world-wide.

Geological background and previous work on the REE mineralization at Palabora

The Palabora Igneous Complex (PCC) is located close to the town of Phalaborwa (South Africa) and intruded at about 2060 Ma into Archaean basement rocks (Reischmann 1995; Wingate and Compston 2000; Heaman 2009; Wu et al. 2011). The complex represents an elongated tripartite pipe-like intrusion divided into a northern and southern pyroxenite and the central Loolekop pipe, with only the latter hosting carbonatites (Fig.1; Hanekom et al. 1965; Yuhara et al. 2003; Verwoerd and du Toit 2006).

The Loolekop pipe is composed of phoscorite (FOS) and Banded Carbonatite (BCB), which are intruded by Transgressive Carbonatite (TCB). Both the BCB and TCB are dolomite-bearing, but calcite-dominated with varying proportions of fluorapatite, phlogopite, magnetite, forsterite/chondrodite and accessory phases (Fig. 2). Geochronological data indicate no significant age differences between these two rock types and Wu et al. (2011) suggest that they crystallized from different magma batches derived from a heterogeneous mantle source. Subsequent injection of a sulphide-rich liquid caused Fe-Cu-sulphide enrichment in the carbonatite pipe (Kavecsanszki et al. 2012). The carbonatite-phoscorite association is surrounded by micaceous pyroxenite (MPY, (Lombaard et al. 1964; Hanekom et al. 1965; Eriksson 1989), several syenite bodies were injected into the surrounding basement rocks in the vicinity of the complex (Eriksson 1989; Yuhara et al. 2003; Wu et al. 2011) and the basement rocks in the border zone towards the complex were fenitized (Verwoerd 1966). The entire complex was cross-cut by dolerite dykes (DOL) which were interpreted as being Proterozoic (Briden 1976; Stettler et al. 1989; Wu et al. 2011) to Post-Karoo (<180 Ma) in age (Hanekom et al. 1965; Uken and Watkeys 1997).

Very similar to what is observed in other carbonatite complexes, apatite represents the main REE host in carbonatites from the PCC and is much higher in REE than calcite and dolomite (Dawson and Hinton 2003). Early investigations on the REE distribution in carbonatites of the PCC suggested the absence of REE minerals (Aldous 1980). Later, bastnäsite, parisite, synchysite, ancylite, monazite, Sr-REE apatite and an unknown REE-silicate were described by Bulakh et al. (1998) and Karchevsky (2000). These studies used the same 5 samples from the open pit level (random sampling - upper 600 meters of the deposit; Bulakh personal communication) and provided only incomplete textural descriptions on their occurrence. Bastnäsite (and minor parisite) was identified as the most abundant REE mineral in the BCB, whereas ancylite (and minor synchysite) was described as the most abundant REE mineral in the TCB. Monazite was described as mainly forming rims around or veins in apatite and an unknown REE-silicate was mentioned to form rims around chondrodite.

Sample material and analytical methods

The Loolekop pipe is divided into three sections: the open pit level (uppermost part), the first lift level (upper underground level) and the second lift level (lowest part, Fig. 1), representing a vertical profile of >1500 m. We collected about 400 samples from 6 drill holes (LK-109, U-2, U-33, MT-1, SL-131, FS-14) and the observations reported in the following derive from 45 representative samples (20 TCB, 15 BCB and 10 FOS) covering all three levels of the Loolekop pipe. All mineral formulae and abbreviations used are given in table 1.

Polished thin sections were investigated using petrographic and reflected-light microscopes and were further examined using the back-scattered electron (BSE) mode (focused beam) of a Hitachi Tabletop SEM (Tübingen), a JEOL JSM-6610 SEM (UFS, Bloemfontein), and the FE-SEM of the Centre for Microscopy (UFS, Bloemfontein).

Quantitative analyses of REE minerals were acquired using a JEOL JXA 8230 Superprobe at the Department of Geology, Rhodes University and a JEOL JXA 8900 Superprobe at the

Department of Geosciences, Eberhard Karls University Tübingen. Data acquisition was performed using four wavelength-dispersive spectrometers. Standardization was done using natural mineral standards, synthetic REE phosphates (SPI Supply) and REE1-4 glasses (Drake and Weill 1972). The ZAF matrix correction method (Bence and Albee 1968; Armstrong 1988) was employed for quantification, except for monazite, where a PRZ (JEOL) correction was used. For analyses of the different REE minerals variable settings were used as detailed in the electronic appendix.

Results

Crystallization sequence of the Palabora carbonatites and phoscorites

Here we provide an overview of the crystallization sequence for carbonatites and phoscorites of the Loolekop deposit. Detailed descriptions of REE minerals (marked red in Fig. 2) are given in the subsequent chapter. The PCC experienced at least four stages of crystallization which were distinguished as (1) orthomagmatic, (2) late-magmatic, (3) sulphide-rich and (4) post-magmatic. Phoscorites (blue field in Fig. 2) are dominated by orthomagmatic minerals, whereas in carbonatites later-magmatic minerals are more common. Although BCB and TCB were classified as two different carbonatites (e.g., Wu et al. 2011), they show some textural differences (from fine banding of mainly magnetite, apatite and phlogopite in BCB to large patchy crystallization of the same minerals in TCB) but generally comprise the same mineral assemblages in the same crystallization sequence. This favors an integration into a single paragenetic scheme together with the phoscorites (Fig. 2).

The orthomagmatic crystallization (stage 1) commenced by the formation of forsterite (with higher abundance in BCB), apatite, baddeleyite (later altered to zirconolite) and thorianite (Figs. 3A-E). Subsequent formation of phlogopite (with higher abundance in BCB; Figs. 3D-F) is followed by magnetite (with minor spinel and ilmenite; Figs. 3G & H), which exsolved further spinel (Figs. 3I & J) and ilmenite (Figs. 3I-K) during later cooling. Precipitation of

153 Mg-rich calcite started during the final stages of apatite formation with its main crystallization
154 phase outlasting that of magnetite. A dolomite formation stage (Fig. 3L) existed
155 contemporaneous with the intermediate stages of calcite formation and during the main calcite
156 stage, additional Sr- and Ba-carbonates formed. Exsolution of dolomite and Mg-poor calcite
157 from Mg-rich calcite (Fig. 3M) concludes the magmatic stage 1.
158 A late-magmatic stage (stage 2) is reflected by the serpentinization (and further magnetite
159 formation) of forsterite (Figs. 6E & F) and replacement of forsterite by chondrodite (Fig. 6G),
160 occasional chloritization of phlogopite (Figs. 6H) and the formation of secondary apatite (ap-
161 II) Stage 2 interweaved with stage 1 and is probably the result of the action of aqueous-
162 carbonic fluids (LM fluid in the following).
163 The subsequent injection of a sulphide-rich liquid (stage 3) resulted in extensive Fe-Cu
164 sulphide mineralization (with minor magnetite). The interaction of a sulphide magma with the
165 carbonatite magma is suspected during this stage (Kavecsanszki et al. 2012).
166 Subsequently, a post-magmatic fluid (stage 4; PM fluid in the following) caused a second
167 serpentinization event (again associated with magnetite), valleriitization of the sulphide
168 minerals (Figs. 6C, D & 8E), recrystallization of carbonates (Fig. 5G; restricted to TCB) and
169 the formation of thorianite, thorite (Figs. 5G & H; restricted to TCB), galena, baryte, celestine
170 (Fig. 7F) and late-stage apatite (ap-III; Figs. 5F & 8F).
171
172 **Textural appearance of REE minerals in the Palabora carbonatites and phoscorites**
173 Ten REE minerals were identified during this study (marked red in Fig. 2; plus the suspected
174 former occurrence of carbocernaite/burbankite), partly occurring in different generations. All
175 REE minerals from the PCC are strongly LREE-enriched (Tab. 2) and typically represent Ce-
176 dominated members, which is displayed by the suffix -(Ce) after the nomenclature of Bayliss
177 and Levinson (1988). The only exception is fergusonite which reflects a Nd-rich endmember
178 (fergusonite-(Nd)-β). Even though the suffix use in mineral nomenclature is recommended by

the Commission on New Minerals, Nomenclature and Classification (CNMNC) of the International Mineralogical Association (IMA), for simplification we abstain from using the suffix in the following.

Fergusonite. The REE-niobate fergusonite (Tab. 2) at the PCC belongs to the Ce-enriched, Nd-dominated endmember of this mineral group and is very rare compared to all other REE minerals found in the Palabora carbonatites. It mostly occurs as rounded to irregular inclusions (max. 80 µm) in magnetite, often associated with baddelyite and zirconolite (Figs. 4A & B).

REE-Ti-betafite (pyrochlore-group member). The REE-Ti-oxide REE-Ti-betafite (alternatively named ceriobetafite; not approved by IMA; Tab 2) seems to be restricted to TCB and represents, after fergusonite, the second rarest REE mineral in the PCC. Betafite requires Ti/(Nb+Ta+Ti) ratios above 1/3, and compositions with Ti>Nb+Ta (Ti-betafite) are very rare and normally exclusively known from granite pegmatites (Yaroshevskii and Bagdasarov 2008). REE-Ti-betafite in the PCC occurs as 25-75 µm sized needles and rods mostly as inclusions in magnetite or, more rarely, in dolomite and calcite (Figs. 4C & D).

REE-F-carbonates. The REE-fluorocarbonates bastnäsite, parisite and synchisite (Tab. 2) are strongly associated with each other, with bastnäsite being by far the most abundant (>80% of all measured REE-F-carbonates). The following three associations can be distinguished:

The first type (REEFC-I) occurs mostly as 10-200 µm sized rods enclosed in magmatic calcite and dolomite (Figs. 5A-C) and is associated with fluorite, strontianite (Fig. 5D) or ancylite (see below). These rods are often partly dissolved and form optically continuous single crystals (Figs. 5A-D). REEFC-I needles partly included in sulphides show a higher resistance for parts protected by the sulphide phase according to the dissolution of these sections (Fig. 5B). The second type (REEFC-II a; restricted to TCB) consists of bastnäsite only that forms bars around monazite replacing apatite and is mostly associated with sulphides, valleriite and

ap-III (Figs. 5E & F). A third type (REEFC-II b; restricted to TCB) consists mainly of bastnäsite and generally occurs as irregularly shaped grains (5-100 µm) in late-stage carbonate veins (Figs. 5G & H). This type is frequently intergrown with magnetite or strontianite and contains inclusions of thorianite and rarely thorite (Figs. 5G & H). In few cases REEFC-II b is associated with anzaite (Fig. 5H).

Monazite. The REE-phosphate monazite (Tab. 2) typically represents La-enriched and Ce-dominated monazite (lanthanian monazite-(Ce) after the nomenclature of Bayliss and Levinson 1988). Monazite is almost always replacing apatite, forming thin skins (≥3 µm) to massive rims (≤40 µm) around the latter (Fig. 6A). These textures can develop to a nearly complete replacement of apatite with tumor-like expansions up to 300 µm in diameter (Fig. 6A). In some cases relics of apatite are surrounded by thick precipitations of monazite (40-300 µm) in cases together with calcite (Fig. 6B). More uncommon appearances include monazite enclosed or in contact with sulphides, which may show reaction rims towards apatite in contact to the reaction of primary sulphide to valleriite (Figs. 6C & D).

Britholite. The Ca-REE-silicate britholite (Tab.2) is mainly present as fluorbritholite-(Ce). Britholite forms rims (≤60 µm thick) around forsterite-serpentine/chondrodite assemblages, where it usually precipitates at the outer rim of the serpentine (Figs. 6E & F) and chondrodite (Fig. 6G). In rare cases britholite (~20 µm thick) is also found in contact with phlogopite/chlorite (Fig. 6H).

Ancylite. The hydrous REE-Sr-carbonate ancylite (Tab.2) occurs in two textural varieties: The first type (ANC-I) forms 15-100 µm sized needles, rods or irregular grains (Figs. 7A-C) that may contain tiny inclusions of baryte (Figs. 7A & B) and are enclosed in calcite and dolomite (in cases associated with REEFC-I). ANC-I is often associated with strontianite and cordylite (see below). A second type (ANC-II) is restricted to TCB and forms 10-50 µm sized grains that are mostly associated with magnetite, strontianite, thorite (Figs. 7D & E) and baryte and rarely occur as crack-fillings together with magnetite and celestine

(Fig. 7F). Similar to REEFC-II b, this type occurs in late carbonate veins, but shows a higher affinity to serpentine, where REE-F-carbonates are usually absent (Figs. 7E & D).

Cordylite. Similar to ANC-I, the REE-Ba-carbonate cordylite (Tab.2) occurs as 10-100 µm sized needles or irregular grains enclosed in calcite and dolomite (Figs. 7G & H). Cordylite is often patchy (Fig. 7H) and may show tails filling tiny veins (Fig. 7G). It was only found in few samples mainly from the uppermost part of the Loolekop pipe, where baryte and celestine are relatively abundant. Importantly, cordylite in direct vicinity to partly dissolved REEFC-I (see above) shows no dissolution or alteration features.

Anzaite. A REE-Ti-oxide rarely found in the PCC is most likely anzaite (Tab. 2), which up to now has only been described from the Afrikanda Complex (Russia; Chakhmouradian et al. 2015). In order to ultimately distinguish anzaite from a cation-deficient perovskite (which has to date not been described from a natural occurrence, though) XRD analyses would be needed (Chakhmouradian et al. 2015). In the investigated samples, anzaite occurs in two distinct associations: (1) In most cases 10-30 µm sized anzaite replaces ilmenite (Figs. 8A-D) and often shows patchy zonation, reflecting variable REE/Ti ratios (Fig. 8A). (2) Mostly in medium to highly serpentinized samples (restricted to TCB), however, 5-30 µm sized irregular grains or schlieren of anzaite occur, which are commonly associated and mostly intergrown with valleriite, but not with ilmenite (Figs. 8E & F).

Discussion

The identification of fergusonite, REE-Ti-betafite, cordylite and britholite during this study represents the first described occurrence of these REE minerals in the PCC and the first occurrence in a carbonatite complex of South Africa. Bulakh et al. (1998) mentioned a Ti-REE mineral and Karchevsky (2000) described a REE-silicate for the PCC, but both gave no further specifications on these minerals. The probable identification of anzaite represents its second occurrence world-wide.

Multi stage formation of REE minerals in the Palabora carbonatites and phoscorites

Most REE mineralizations in carbonatites are believed to have crystallized from carbo- or hydrothermal fluids (e.g., Mariano 1989; Wall and Mariano 1996; Wyllie et al. 1996; Wall et al. 2001; Zaitsev et al. 2002; Williams-Jones et al. 2012; Nadeau et al. 2015). However, fluid inclusion studies show that REE do not preferentially fractionate into fluids, although they would be capable in transporting REE (Bühn and Rankin 1999). Experimental studies at high temperatures (Song et al. 2016) imply that carbonatite-related REE deposits may form by fractional crystallization of carbonatitic melts rather than from exsolved hydrothermal fluids. In rare cases only, a magmatic origin for REE mineralizations in carbonatites is assumed, based on textural (e.g., Mountain Pass, Mariano 1989) and isotopic data (e.g., Zaitsev et al. 2002) with alteration, replacement and remobilization of preexisting REE minerals clearly linked to a late-stage process involving water-bearing fluids (e.g., Wall and Mariano 1996; Zaitsev et al. 1998; Wall et al. 2001; Zaitsev et al. 2002; Moore et al. 2015). Some paragenetic studies on individual carbonatite complexes indicate multistage mineralization processes with significant overprint of the orthomagmatic mineralization by a late-stage hydrothermal or carbothermal mineralization (Rankin 2005). Nevertheless, the controls on the REE mineralization in carbonatites are poorly understood (Trofanenko et al. 2016).

Based on the textures described above, the various REE mineral associations at Palabora formed during different stages (Figs. 2 & 9): Whilst fergusonite, REE-Ti-betafite and probably also REEFC-I crystallized during the orthomagmatic stage directly from a carbonatitic melt, monazite and britholite precipitated from late-magmatic fluids (LM fluid). Finally, the formation of anzaite, REEFC-II (a+b) and ANC-II and the alteration of monazite and REEFC-I is assigned to REE redistribution processes caused by post-magmatic fluids (PM fluid). Although the genetic position of ANC-I and cordylite is not entirely clear, the

association with baryte and the integrity of ANC-I and cordylite needles next to strongly dissolved REEFC-I needles favor a formation during stage 4 (Fig. 2).

The variability of types of REE mineralization in the PCC largely reflects the sensitive character of REE mineral formation during fluid-assisted processes. We suggest that late-magmatic and post-magmatic fluids show compositional variabilities, which are probably caused by local dissolution-reprecipitation processes. We distinguish the following fluid types: LM = late-magmatic fluid enriched in REE, LM′ = REE-depleted analogue of LM that results from REE mineral precipitation from LM, PM = post-magmatic REE-poor or -free initial fluids, PM′ = fluids enriched in REE by remobilization, PM′′ = REE- and cation-enriched fluids transporting the element content for distal precipitation, and PM′′′ = REE-depleted fluids after REE mineral precipitation from PM′ and PM′′.

Orthomagmatic crystallization of fergusonite, REE-Ti-betafite and REE-F carbonates

Texturally, fergusonite and REE-Ti-betafite are interpreted as early magmatic REE phases, which probably crystallized more or less contemporaneously. Fergusonite represents the most important Nb-phase in the system (pyrochlore sensu stricto is lacking), but its very low abundance reflects a general depletion of Nb in the Palabora carbonatites. Hence, the PCC comprises a magmatic association of a Ti-poor Nb-oxide (fergusonite; <0.13wt% TiO_2) and a Nb-poor Ti-oxide (REE-Ti-betafite; < 0.11wt% Nb_2O_5). Notably, Ti-bearing fergusonite (>1 wt% TiO_2) and Nb-bearing betafite (up to 20 wt% Nb_2O_5) were described (e.g., Mitchell and Chakhmouradian 1998; Tomašić et al. 2006; Yaroshevskii and Bagdasarov 2008). At this stage it remains unclear, why magmatic fergusonite and betafite in the PCC do not incorporate significant amounts of Ti and Nb, respectively. The enclosure of both mineral phases in magnetite isolates these minerals mostly from later fluid interactions and alteration (Fig. 9).

In general, REE-fluorocarbonates are among the most abundant REE minerals in carbonatites (Shunhua et al. 1986; Hsu 1992; Williams-Jones and Wood 1992). Although REE-F-

carbonates (especially bastnäsite) are stable to temperatures above 600°C (Wyllie et al. 1996 and references therein), most REE-fluorocarbonates precipitate at comparatively low temperatures (Williams-Jones and Wood 1992). Magmatic REE-F-carbonates (mainly represented by bastnäsite) from Mountain Pass were described as coarse-grained hexagonal prismatic (strongly elongated) crystals in fine- to medium-grained calcite and baryte, while fine-grained stubby hexagonal interstitial prisms of bastnäsite were formed by a late residual fluid (Castor 2008).

At Palabora REE-F-carbonates (REEFC-I) occur as small and elongated crystals that are partly dissolved and form optically continuous single crystals (Fig. 5A & B) and well-preserved REEFC-I needles are included in sulphides. Based on this and the similarities to REE-F-carbonates at Mountain Pass (except for crystal size), we assume a magmatic origin for REEFC-I at Palabora.

Normally REE-F-carbonates contain minor amounts of Th (e.g., Armbrustmacher 1979; Smith et al. 2000; Humphries 2012). For example, bastnäsite typically contains 0.2-0.3 wt% thorium (Wang et al. 2013) and can also occur as thorbastnäsite (Smith et al. 2000) with 47 wt% Th (Pavlenko et al. 1965). Uher et al. (2015) even report ThO_2 concentrations of 0.5 to 1.4 wt% for bastnäsite and 0.4 to 4.5 wt% for synchysite in a granite at Stupné, Slovakia. In our case, REEFC-I are Th-poor (<0.08 wt%), which is in contrast to REEFC-II (see below). We suggest that early magmatic precipitation of Th-minerals (mostly thorianite; Figs. 2 & 3B), caused an early depletion of Th in the magmatic system, which resulted in lower Th concentrations during the stage of REEFC-I precipitation. Furthermore, partly dissolved REEFC-I (Fig. 5A) indicates a later remobilization of REE and the patchy appearance of parisite and synchysite within the bastnäsite interdigitation indicates an alteration of bastnäsite to synchysite and parisite during the remobilization of REE (see below).

Late-magmatic formation of monazite and britholite at the expense of apatite and forsterite

Monazite formation. The replacement of apatite by monazite has been described for some hydrothermal deposits (e.g., Pan et al. 1993a; Lieftink et al. 1994; Smith et al. 1999) as a late-stage alteration phenomenon (Wall and Mariano 1996). Monazite inclusions and rims around apatite are often explained by fluid-induced (metasomatic) alteration of apatite via coupled substitution and mass transfer (Harlov et al. 2002; Harlov and Förster 2003; Harlov et al. 2005). As such, monazite may have originated from the REE budget available from apatite itself, Si and Na would be removed from the apatite without concurrent removal of REE (Pan et al. 1993a; Harlov and Förster 2002; Harlov et al. 2002).

In the investigated samples there is no textural evidence to suggest that monazite is the result of exsolution from precursor apatite during cooling. Rather, apatite shows strong dissolution textures and mass balance considerations imply that the REE content of the apatite is not sufficient to allow for the precipitation of the observed amounts of monazite (Figs. 6A & B). We suggest that the precipitation of monazite (in cases associated with calcite) at the expense of apatite was caused by a REE-bearing fluid, according to the following schematic equation:

Apatite + LM Fluid = Monazite + Calcite + LM´ Fluid

$$Ca_5(PO_4)_3F + CO_3^{2-} + 3REE^{3+} = 3REE(PO_4) + CaCO_3 + F^- + 4Ca^{2+} \quad [1]$$

Due to the relative immobility of phosphate (Smith et al. 1999; Poitrasson et al. 2004; Cetiner et al. 2005; Louvel et al. 2015), monazite mainly precipitates directly at the contact to apatite or within its immediate vicinity. The different appearances from surficial dissolution (thin skins of monazite around euhedral apatite; Fig. 6A) to nearly complete dissolution (larger masses of monazite with just relict apatite; Fig. 6B) probably reflect variable degrees of apatite replacement by monazite linked to the degree of apatite dissolution by the fluid.

Britholite formation. Britholite is mainly described from nepheline syenites and contact metasomatic deposits, where it generally forms during hydrothermal processes related to the replacement of apatite or monazite (Budzyń et al. 2011; Uher et al. 2015; Zirner et al. 2015). Britholite was also described as a low-temperature phase in the Virulando carbonatite (Angola) formed at late-stage supergene alteration processes, associated with synchysite, cerite, goethite, hollandite and baryte (Torró et al. 2012). In all, britholite is assumed to have a late stage to post-magmatic (subsolidus alteration of primary minerals) origin for most occurrences (Wall et al. 1993; Uher et al. 2015).

Typically, britholite obtains the necessary anions from Si-bearing hydrothermal fluids. However, because of a general lack of Si-rich fluids in carbonatitic systems, another Si source has to be considered. Based on textural evidence, we suggest that Si is provided by the serpentinization of forsterite and the replacement of forsterite by chondrodite to which britholite is largely bound (Fig. 6F, G & 9). As forsterite is REE-poor, the britholite-forming fluid contained appreciable amounts of REE, in accordance with the assumptions made for monazite formation above:

Forsterite + LM Fluid = Serpentine + Dolomite + Britholite + LM´ Fluid

$$9Mg_2SiO_4 + 3½H_2O + 5½H^+ + ½F^- + 4Ca^{2+} + 4CO_3^{2-} + 3REE^{3+} =$$

$$3Mg_3Si_2O_5(OH)_4 + 2MgCa(CO_3)_2 + Ca_2(REE)_3(SiO_4)_3(F,OH) + 7Mg^{2+} \quad [2]$$

Forsterite + LM Fluid = Chondrodite + Britholite + LM´ Fluid

$$5Mg_2SiO_4 + ⅔Ca^{2+} + 4⅓F^- + REE^{3+} =$$

$$2Mg_5(SiO_4)_2F_2 + ⅓Ca_2(REE)_3(SiO_4)_3(F) \quad [3]$$

In few cases britholite formation is associated with the chloritization of phlogopite:

Phlogopite + LM Fluid = Chlorite + Britholite + LM´ Fluid

385 $2KMg_3(Si_3Al)O_{10}(F_2) + 10OH^- + 2Ca^{2+} + 3REE^{3+} =$

386 $(Mg_5Al)(Si_3Al)O_{10}(OH)_8 + Ca_2(REE)_3(SiO_4)_3(F) + Mg^{2+} + 2K^+ + 3F^- + 2H^+$ *[4]*

387

388 Although britholite from Palabora is generally F-rich (fluorbritholite; Fig. 10 II), britholite
389 associated with the replacement of forsterite by chondrodite and the chloritization of
390 phlogopite is higher in F than the britholite associated with the serpentinization of forsterite.
391 This shows that the LM fluid contains variable contents of F (Fig. 10 II).
392 Based on textural observations (Figs. 6E), we suggest that monazite and britholite formed
393 contemporaneously from the same fluid (Fig. 9). Accordingly, the type of REE phase formed
394 depends on the local presence of forsterite or apatite, which provide the necessary anions
395 SiO_4^{4-} or PO_4^{3-}, respectively. The occasional presence of acicular ap-II in serpentine indicates
396 that small amounts of P (released by monazite formation; confirmed by mass balance
397 calculations; or dissolution of apatite) may cause precipitation of secondary apatite during
398 serpentinization of forsterite. The absence of REE in olivine and too low concentrations in
399 apatite indicates the necessity to import REE into the system to precipitate britholite and
400 monazite (arrows labelled [1] – [3] in Fig. 10).

401

402 **Post magmatic redistribution of REE: formation of cordylite, ancylite, REE-F**
403 **carbonates and anzaite**

404 **Cordylite and ancylite (ANC-I) formation**. Whereas ancylite is a relatively common REE
405 mineral in carbonatites, cordylite is extremely rare (Zaitsev et al. 1998). Ancylite has never
406 been described as a primary magmatic mineral, rather it is specified as a useful indicator of
407 hydrothermal/carbothermal processes (Wall and Zaitsev 2004a; Verplanck et al. 2016).
408 Zaitsev et al. (1998) describe the association of cordylite and ancylite as resulting from the
409 hydrothermal alteration of magmatic carbocernaite and burbankite. Based on this and our own
410 textural observations (see above), we suggest that cordylite (Fig. 7G) and ANC-I (Figs. 7A-C;

411 together with baryte and strontianite with which it is tightly associated) may replace precursor
412 REE-Ca-Sr-carbonates. Because of the absence of any relics it is not possible to identify the
413 precursor mineral of cordylite and ANC-I. However, based on very similar textural
414 descriptions in the literature (Pecora and Kerr 1953; Somina 1975; Kapustin 1980; Zaitsev et
415 al. 1998; Moore et al. 2015) we assume the former presence of carbocernaite/burbankite (red
416 question mark in fig. 2). Burbankite and/or carbocernaite are important REE minerals in
417 carbonatites that were probably present in many carbonatites but are typically replaced by
418 ancylite, strontianite, synchysite, calcite, baryte, quartz, monazite and apatite (e.g.,
419 Kangankunde, Malawi; Wigu Hill, Tanzania; Adiounedj, Mali; Bear Lodge, Wyoming and
420 Gem Park, USA; Wall et al. 1997). Supposing the precipitation of cordylite and ancylite
421 during the early phase of stage 4 (Fig. 2 & 9), we suggest that dissolution of REEFC-II (see
422 below) controls the activity of F in the fluid, which in turn controls the formation of ancylite
423 and cordylite (Fig. 10 III). Ancylite and cordylite are depleted in Th, suggesting that the fluid
424 from which they precipitated from was also Th-poor. The later precipitation of secondary
425 thorianite and thorite as well as slightly higher Th contents in later secondary REE minerals
426 suggest Th-enrichment of the fluid by dissolution of primary Th minerals.

427 **Monazite alteration.** Monazite in contact with or enclosed by sulphides is
428 occasionally altered to ap-III associated with the valleriitization of the sulphide (Fig. 6C & D,
429 9). This may be caused by the remobilization of REE from monazite (Fig. 10 I) by the same
430 fluid that caused valleriitization of sulphides and can be explained by the following schematic
431 equation:

432

433 Monazite + Chalcopyrite + PM Fluid = Apatite + Valleriite + PM´ Fluid

434 $3REE(PO_4) + CuFeS_2 + 5Ca^{2+} + HF + Mg^{2+} + ½Al^{3+} + 2OH^- =$

435 $Ca_5(PO_4)_3F + 2((Fe,Cu)S)\cdot 1.53(Mg,Al)(O,OH)_2) + 3REE^{3+} + 2½H^+$ *[5]*

436

437 Valleriitization in association with ap-III formation sometimes includes thorite (Fig. 6D),
438 which is supposed to be formed by the remobilization of Th from primary Th minerals by the
439 post-magmatic fluid.

440 **REEFC-II formation.** REEFC-II show two different types of occurrence, which may
441 be distinguished into a proximally (REEFC-II a) and a distally precipitated (REEFC-II b)
442 variety depending on the REE saturation of the fluid (Fig. 9). The proximal variety (Figs. 5E
443 & F) indicates reaction of monazite, apatite and a fluid, which is linked to reaction *5* with the
444 exception of the availability of CO_3^{2-} by the dissolution of carbonate. The remobilization of
445 REE during this reaction will be prevented by the formation of REEFC-II a (exclusively
446 bastnäsite), similar to what was observed in the Bayan Obo deposit (Smith et al., 1999):
447
448 Monazite + Calcite + PM Fluid = Apatite + Bastnäsite + PM´ Fluid
449 $3(REE)PO_4 + 5CaCO_3 + 4HF = Ca_5(PO_4)_3F + 3(REE)(CO_3)F + 2H_2O + 2CO_2$ *[6]*
450
451 Partial dissolution of REEFC-I (see above) may form strontianite, parisite/synchysite and
452 fluorite in the interstices of the REEFC-I interdigitation (Fig. 5D & 9). This may cause
453 additional remobilization of REE by the evacuation of dissolved components ($(REE)(CO_3)F$
454 $\leftrightarrow REE^{3+} + CO_3^{2-} + F^-$). The alteration of REEFC-I to parisite and synchysite may be caused
455 by interaction with a Ca-rich fluid, while the presence of Sr promotes additional precipitation
456 of strontianite and fluorite:
457
458 Bastnäsite + PM Fluid = Parisite
459 $2(REE)(CO_3)F + Ca^{2+} + CO_3^{2-} = Ca(REE)_2(CO_3)_3F_2$ *[7]*
460
461 Bastnäsite + PM Fluid = Strontianite + Parisite + Fluorite + PM´ Fluid
462 $4(REE)(CO_3)F + 2Ca^{2+} + Sr^{2+} = SrCO_3 + Ca(REE)_2(CO_3)_3F_2 + CaF_2 + 2REE^{3+}$ *[8]*

463

464 The observation that REEFC-I needles, protected by sulphide encapsulation (Fig. 5B), do not
465 show the described alteration indicates that this process happens after the formation of
466 sulphide minerals and during the post-magmatic stage.
467 The second variety (distal; REEFC-II b) precipitated in vein-like fluid paths together with
468 secondary strontianite, magnetite, anzaite, valleriite, thorianite and thorite (Figs. 5G & H &
469 9). Thus, the fluid causing the precipitation of these secondary minerals was probably
470 enriched in Th. Thorium can be remobilized by leaching and dissolution of primary thorium-
471 bearing minerals such as thorianite (Pan et al. 1993b). At high temperatures, Th can be
472 incorporated into REE minerals (Harlov et al. 2011), whereas at low temperatures, Th
473 incorporation into REE minerals is restricted (Read et al. 2002; Doroshkevich et al. 2008;
474 Budzyń et al. 2010), explaining the coexistence of secondary Th minerals with REEFC-II b
475 (Figs. 5G & H). In fact, Th contents in REEFC-II are higher than in REEFC-I, but the
476 depletion of Th in REEFC-I depends on the depletion of Th in the melt during REEFC-I
477 precipitation after the early crystallization of Th minerals (see above), while REEFC-II b
478 formed concurrently with Th minerals due to the remobilization of Th from primary Th
479 minerals. Formation of REEFC-II b may have occurred according to the following schematic
480 reactions:

481

482 Dolomite A + Calcite A + PM′ Fluid =

483 REEFC-II b (Bastnäsite) + Calcite B + Dolomite B + PM′′′ Fluid

484 $2MgCa(CO_3)_2 + CaCO_3 + REE^{3+} + HF =$

485 $REE(CO_3)F + 2CaCO_3 + MgCa(CO_3)_2 + Mg^{2+} + H^+$ *[9]*

486

The percolating fluid that caused the formation of REEFC-II b further induced dissolution (calcite A & dolomite A) and recrystallization (calcite B & dolomite B) of carbonates constituting a further generation of carbonates within veins (Fig. 5G).

Ancylite (ANC-II) formation. Similarly, ANC-II is bound to vein-like fluid paths with a secondary mineralization of carbonates (Fig. 7D). However, ANC-II was not observed to coexist with REEFC-II b. Rather, in cases where REEFC-II b are present, the dominant Sr phase is REE-poor strontianite ($\sum REE_2O_3$ < 4wt%; Karchevsky 2000) and REE are mainly incorporated into REEFC-II b (Fig. 9). At presumably higher H_2O activities, the formation of serpentine and the absence of the REEFC-II b lead to REE concentration into the Sr phase ancylite. The necessary Sr was probably provided by the dissolution of strontianite and/or Sr-rich calcite (which occurs as secondary exsolutions in exsolved dolomite):

Dolomite A + Calcite A + Strontianite + PM′ Fluid =

ANC-II + Dolomite B + Calcite B + PM′′′ Fluid

$$MgCa(CO_3)_2 + 2¼CaCO_3 + ¾SrCO_3 + 2H_2O + REE^{3+} =$$

$$(Sr_{0.75}Ca_{0.25})(REE)(CO_3)_2(OH)\cdot H_2O + MgCa(CO_3)_2 + CaCO_3 + Ca^{2+} + H^+ \quad [10]$$

Dolomite A + Sr-Calcite + PM′ Fluid = ANC-II + Dolomite B + Calcite + PM′′′ Fluid

$$MgCa(CO_3)_2 + 3(Ca_{0.75}Sr_{0.25})CO_3 + 2H_2O + REE^{3+} =$$

$$(Sr_{0.75}Ca_{0.25})(REE)(CO_3)_2(OH)\cdot H_2O + MgCa(CO_3)_2 + CaCO_3 + Ca^{2+} + H^+ \quad [11]$$

Anzaite formation. Anzaite-(Ce) was first described from Afrikanda (Russia) as a late hydrothermal alteration product where Ti and Fe were derived from primary Ti oxides such as ilmenite, which is reflected by a ubiquitous association of anzaite with ilmenite and/or Ti-rich magnetite (Chakhmouradian et al. 2015). The associated mineral assemblage precipitated at Afrikanda at 150-250°C, $aH^{+} \approx 10^{-5}$ and $aH_4SiO_4^0 > 10^{-4}$ (Chakhmouradian and Zaitsev 2004). The close association of anzaite with valleriite (Figs. 8E & F) at Palabora confirms the assumption of a low-temperature origin. Anzaite is texturally bound to ilmenite (Figs. 8B & D). Therefore, the partial dissolution of ilmenite by a REE-bearing fluid seems to be essential for the local enrichment of Ti allowing for the formation of anzaite. Two different occurrences of anzaite can be distinguished, which might reflect a proximal and distal fluid transport (Fig. 9) of a Ti-enriched REE-bearing fluid:

The common association includes anzaite with relics of ilmenite in direct contact or close vicinity with magnetite (Figs. 8A-D). In this case, anzaite directly replaces ilmenite, which can be described by the following schematic equation:

Ilmenite + PM′ Fluid = Anzaite + PM′′′ Fluid

$$6FeTiO_3 + 2OH^- + 4REE^{3+} = REE_4FeTi_6O_{18}(OH)_2 + 5Fe^{2+} \quad [12]$$

The less common occurrence of anzaite is not directly bound to ilmenite but associated with valleriite and serpentine (Fig. 8E & F). This association requires small-scale hydrothermal transport of Ti, Al and Si by a REE-bearing fluid. In general, very low pH combined with the availability of complexing ligands such as F can enable Ti transport in fluids (Van Baalen 1993). However, we consider such low pH values (<2) unlikely for the studied environment. Alternatively, significant mass transfer of Ti was explained by complexing agents of polymerized silicate molecules in solution (Manning 2004), most likely Ti-aluminosilicate complexes (Tropper and Manning 2005; Beitter et al. 2008). We favor this explanation as the

533 assumption of the existence of Ti-transporting aluminosilicate complexes provides Al and Si
534 for valleriite and serpentine formation, respectively (as observed; reaction *13b*). The
535 precipitation of this type of anzaite together with valleriite may be expressed by a two-step
536 process. First, ilmenite is dissolved and Ti-aluminosilicate-complexes form:
537
538 Ilmenite + PM′ Fluid (incl. aluminosilicate-complex) = PM′′ Fluid
539 $FeTiO_3 + 6⅓OH^- + 3H_2O + 7Mg^{2+} + 2AlOSi(OH)_3^{2+} + ⅔REE^{3+} =$
540 $12⅓OH^- + 7Mg^{2+} + 2(Ti,Fe)\text{-}AlOSi(OH)_3^{5+} + ⅔REE^{3+}$ *[13a]*
541
542 This Ti-enriched fluid may then precipitate anzaite together with valleriite and serpentine
543 when getting in contact with sulphides:
544
545 PM′′ Fluid + Cu-Fe Sulphide (e.g., Chalcopyrite) =
546 Anzaite + Valleriite + Serpentine + PM′′′ Fluid
547 $12⅓OH^- + 7Mg^{2+} + 2(Ti,Fe)\text{-}AlOSi(OH)_3^{5+} + ⅔REE^{3+} + 4CuFeS_2 =$
548 $⅙REE_4FeTi_6O_{18}(OH)_2 + 4(2((Fe,Cu)S)\cdot 1.53((Mg,Al)(O,OH)_2)) + ½Mg_6Si_4O_{10}(OH)_8$
549 $+ ⅚Fe^{2+} + 12H^+$ *[13b]*
550
551 The type of anzaite formation (proximal or distal; Fig. 9) depends on the availability of
552 potential Ti-complexing ligands and is therefore locally controlled by the earlier enrichment
553 of Si and Al.
554 Although Kavecsanszki et al. (2012) assume that the sulphide-bearing liquid (stage 3)
555 released fenitizing fluids, the actual source of the PM fluid is not demonstrated yet.
556 Alternatively, external fluids, e.g., related to the cross-cutting dolerite dykes, may have
557 caused post-magmatic alteration reactions within the carbonatites.
558

Implications

Variable textures involving REE minerals from the Palabora Carbonatite Complex record their multi-stage formation. Some REE minerals exhibit different generations that formed during different evolutionary stages and the REE mineral assemblages that formed after the orthomagmatic stage are controlled by the precursor mineralogy and fluid composition. There is a complex interplay between host minerals, fluid chemistry and REE mineralogy after the orthomagmatic stage. This interplay leads to a variety of local chemical (micro)environments reflected in different REE mineral assemblages.

Our results suggest that hydrothermal processes during late-magmatic and post-magmatic stages are of greater importance with respect to the formation and variability of REE minerals than orthomagmatic crystallization. Hydrothermal overprint causes alteration and in cases complete replacement of primary REE minerals. Our study on the Palabora carbonatites further implies that the REE contents of magmatic minerals (such as apatite and carbonates) are not high enough to account for the formation of late-magmatic REE minerals such as monazite, which suggests that a REE-enriched fluid was introduced into the observed sections of the complex during late-magmatic stages.. The results of this study confirm (i) the significance of late-stage introduction of REE and their reaction with precursor mineral phases and (ii) the redistribution of REE during post-magmatic stages in natural carbonatitic systems.

Acknowledgements

Anatoly N. Zaitsev is thanked for helpful comments on an earlier version of our manuscript. We thank Glen Taylor (Director of Research UFS) for providing funds for the visits in RSA as well as the stays at Phalaborwa and the DFG for general funding of this project (MA 2563/10-1). The Department of Geology at the University of the Free State is acknowledged for making the FE-SEM (Pieter van Wyk) and SEM available, to continuously facilitate

585 contact to PMC (operating company at Palabora) and for several discussions. Furthermore we
586 want to thank PMC for providing core material and the help during our different sampling
587 campaigns.
588 In a special way we would like to remember Pavel I. Karchevsky (1976-2002) whose study
589 about the rare earth mineralization of the PCC was a significant cornerstone for our work.
590

591 **References cited**

592 Aldous, R. T. H. (1980) Ore genesis in copper bearing carbonatites: a geochemical, fluid
593 inclusion and mineralogical study, 365 p. Ph.D. thesis, Imperial College London
594 (University of London), London.
595 Armbrustmacher, T. J. (1979) Replacement and primary magmatic carbonatites from the Wet
596 Mountains area, Fremont and Custer counties, Colorado. Economic Geology, 74, 888-
597 901.
598 Armstrong, J. T. (1988) Bence-Albee after 20 years: review of the accuracy of a-factor
599 correction procedures for oxide and silicate minerals. Microbeam Analysis,
600 Applications in Geology, 469-476.
601 Bayliss, P., and Levinson, A. A. (1988) A system of nomenclature for rare-earth mineral
602 species: revision and extension. American Mineralogist, 73, 93-99.
603 Beitter, T., Wagner, T., and Markl, G. (2008) Formation of kyanite–quartz veins of the Alpe
604 Sponda, Central Alps, Switzerland: implications for Al transport during regional
605 metamorphism. Contributions to Mineralogy and Petrology, 156, 689-707.
606 Bence, A. E., and Albee, A. L. (1968) Empirical correction factors for the electron
607 microanalysis of silicates and oxides. The Journal of Geology, 76, 382-403.
608 Briden, J. C. (1976) Application of palaeomagnetism to Proterozoic tectonics. Philosophical
609 Transactions of the Royal Society of London A: Mathematical, Physical and
610 Engineering Sciences, 280, 405-416.

611 Budzyń, B., Hetherington, C. J., Williams, M. L., Jercinovic, M. J., and Michalik, M. (2010)
612 Fluid− mineral interactions and constraints on monazite alteration during
613 metamorphism. Mineralogical Magazine, 74, 659-681.
614 Budzyń, B., Harlov, D. E., Williams, M. L., and Jercinovic, M. J. (2011) Experimental
615 determination of stability relations between monazite, fluorapatite, allanite, and REE-
616 epidote as a function of pressure, temperature, and fluid composition. American
617 Mineralogist, 96, 1547-1567.
618 Bulakh, A. G., Rudashevsky, N. S., and Karchevsky, P. I. (1998) Native gold and silver,
619 sulfides and REE minerals in carbonatites from Loolekop Deposit, South Africa.
620 Zapiski Vserossijskogo Mineralogiceskogo Obscestva, 127, 45-54.
621 Castor, S. B. (2008) The Mountain Pass rare-earth carbonatite and associated ultrapotassic
622 rocks, California. The Canadian Mineralogist, 46, 779-806.
623 Cetiner, Z. S., Wood, S. A., and Gammons, C. H. (2005) The aqueous geochemistry of the
624 rare earth elements. Part XIV. The solubility of rare earth element phosphates from 23
625 to 150 C. Chemical geology, 217, 147-169.
626 Chakhmouradian, A. R., and Wall, F. (2012) Rare earth elements: minerals, mines, magnets
627 (and more). Elements, 8, 333-340.
628 Chakhmouradian, A. R., and Zaitsev, A. N. (2004) Afrikanda: An association of ultramafic,
629 alkaline and alkali-silica-rich carbonatitic rocks from mantle-derived melts.
630 Phoscorites and carbonatites from mantle to mine: the key example of the Kola
631 Alkaline Province, Mineralogical Society (UK) Series, 10, 247-291.
632 Chakhmouradian, A. R., and Zaitsev, A. N. (2012) Rare earth mineralization in igneous rocks:
633 sources and processes. Elements, 8, 347-353.
634 Chakhmouradian, A. R., Cooper, M. A., Medici, L., Abdu, Y. A., and Shelukhina, Y. S.
635 (2015) Anzaite-(Ce), a new rare-earth mineral and structure type from the Afrikanda
636 silicocarbonatite, Kola Peninsula, Russia. Mineralogical Magazine, 79, 1231-1244.

637 Dawson, J. B., and Hinton, R. W. (2003) Trace-element content and partitioning in calcite,
638 dolomite and apatite in carbonatite, Phalaborwa, South Africa. Mineralogical
639 Magazine, 67, 921-930.
640 Doroshkevich, A. G., Ripp, G. S., Viladkar, S. G., and Vladykin, N. V. (2008) The Arshan
641 REE carbonatites, southwestern Transbaikalia, Russia: mineralogy, paragenesis and
642 evolution. The Canadian Mineralogist, 46, 807-823.
643 Drake, M. J., and Weill, D. F. (1972) New rare earth element standards for electron
644 microprobe analysis. Chemical geology, 10, 179-181.
645 Eriksson, S. C. (1989) Phalaborwa: a saga of magmatism, metasomatism and miscibility. In
646 K. Bell, Eds., Carbonatites: genesis and evolution. , p. 221-254. Unwin Hyman,
647 London.
648 European-Commission (2014) Report on critical raw materials for the EU—report of the Ad
649 hoc Working Group on defining critical raw materials.
650 Fernandez, A. L. I., Doval, M., and Lopez-Aguayo, F. (1977) Thermal behavior of valleriite.
651 American Mineralogist, 62, 1030-1031.
652 Fleet, M. E. (2006) Phase equilibria at high temperatures. In D. J. Vaughan, Eds., Sulphide
653 Mineralogy and Geochemistry, p. 365-419. Reviews in Mineralogy and Geochemistry,
654 Mineralogical Society of America, Chantilly, Virginia.
655 Fourie, P. J., and De Jager, D. H. (1986) Phosphate in the Phalaborwa complex. Mineral
656 Deposits of Southern Africa, 2, 2239-2253.
657 Hanekom, H. J., Van Staden, C. M. V. H., Smit, P. J., and Pike, D. R. (1965) The geology of
658 the Palabora igneous complex, 185 p. South African Geological Survey, Pretoria.
659 Harlov, D. E., and Förster, H.-J. (2002) High-grade fluid metasomatism on both a local and a
660 regional scale: the Seward peninsula, Alaska, and the Val Strona di Omegna, Ivrea–
661 Verbano Zone, Northern Italy. Part I: petrography and silicate mineral chemistry.
662 Journal of Petrology, 43, 769-799.

663 Harlov, D. E., and Förster, H.-J. (2003) Fluid-induced nucleation of (Y+ REE)-phosphate
664 minerals within apatite: Nature and experiment. Part II. Fluorapatite. American
665 Mineralogist, 88, 1209-1229.
666 Harlov, D. E., Förster, H.-J., and Nijland, T. G. (2002) Fluid-induced nucleation of (Y+
667 REE)-phosphate minerals within apatite: Nature and experiment. Part I. Chlorapatite.
668 American Mineralogist, 87, 245-261.
669 Harlov, D. E., Wirth, R., and Förster, H.-J. (2005) An experimental study of dissolution–
670 reprecipitation in fluorapatite: fluid infiltration and the formation of monazite.
671 Contributions to Mineralogy and Petrology, 150, 268-286.
672 Harlov, D. E., Wirth, R., and Hetherington, C. J. (2011) Fluid-mediated partial alteration in
673 monazite: the role of coupled dissolution–reprecipitation in element redistribution and
674 mass transfer. Contributions to Mineralogy and Petrology, 162, 329-348.
675 Hatch, G. P. (2012) Dynamics in the global market for rare earths. Elements, 8, 341-346.
676 Heaman, L. M. (2009) The application of U–Pb geochronology to mafic, ultramafic and
677 alkaline rocks: an evaluation of three mineral standards. Chemical geology, 261, 43-
678 52.
679 Hsu, L. C. (1992) Synthesis and stability of bastnaesites in a part of the system (Ce, La)-F-H-
680 C-O. Mineralogy and Petrology, 47, 87-101.
681 Humphries, M. (2012). Report R41347. Congressional Research Service.
682 Kanazawa, Y., and Kamitani, M. (2006) Rare earth minerals and resources in the world.
683 Journal of Alloys and Compounds, 408, 1339-1343.
684 Kapustin, Y. L. (1980) Mineralogy of carbonatites, 259 p. Amerind Publishing Company,
685 New Delhi.
686 Karchevsky, P. I. (2000) Minerals of Sr and REE in carbonatites from Loolekop deposit
687 (Palabora, RSA). Zapiski Vserossijskogo Mineralogiceskogo Obscestva, 129, 99-109.

688 Kavecsanszki, D., Moore, K. R., Rollinson, G. K., Wall, F., and Lusty, P. a. J. (2012) Magma
689 mingling between sulphide-rich and carbonatite magmas to form a multi-commodity
690 metal deposit: reconstruction using QUEMSCAN analysis. In E. Jonsson, Eds.,
691 Proccdings of the Conference Proceedings. 12th SGA Biennial Meeting: Mineral
692 deposit research for a high tech world, p.1024-1027. Uppsala, Sweden.
693 Lieftink, D. J., Nuland, T. G., and Maijer, C. (1994) The behavior of rare earth elements in
694 high-temperature Cl-bearing aqueous fluids: Results from the Odegardens Verk
695 Natural Laboratory. The Canadian Mineralogist, 32, 149-158.
696 Lombaard, A. F., Ward-Able, N. M., and Bruce, R. W. (1964) The exploration and main
697 geological features of the copper deposit in carbonatite at Loolekop, Palabora
698 complex. In Eds., The geology of some ore deposits in southern Africa, p. 315-337.
699 Geological Society of South Africa, Johannesburg.
700 Louvel, M., Bordage, A., Testemale, D., Zhou, L., and Mavrogenes, J. (2015) Hydrothermal
701 controls on the genesis of REE deposits: Insights from an in situ XAS study of Yb
702 solubility and speciation in high temperature fluids (T< 400° C). Chemical geology,
703 417, 228-237.
704 Manning, C. E. (2004) Polymeric silicate complexing in aqueous fluids at high pressure and
705 temperature, and its implications for water-rock interaction. In R. B. Wanty & R. R.
706 Seal II, Eds., Water-Rock Interactions, p. 45-49. Balkema, New York.
707 Mariano, A. N. (1989) Nature of economic mineralization in carbonatites and related rocks. In
708 K. Bell, Eds., Carbonatites: genesis and evolution, p. 149-176. Unwin Hyman,
709 London.
710 Mitchell, R. H., and Chakhmouradian, A. R. (1998) Th-rich loparite from the Khibina alkaline
711 complex, Kola Peninsula: isomorphism and paragenesis. Mineralogical Magazine, 62,
712 341-353.

713 Moore, M., Chakhmouradian, A. R., Mariano, A. N., and Sidhu, R. (2015) Evolution of rare-
714 earth mineralization in the Bear Lodge carbonatite, Wyoming: Mineralogical and
715 isotopic evidence. Ore Geology Reviews, 64, 499-521.
716 Nassar, N. T., Du, X., and Graedel, T. (2015) Criticality of the rare earth elements. Journal of
717 Industrial Ecology, 19, 1044-1054.
718 Pan, Y., Fleet, M. E., and Macrae, N. D. (1993a) Oriented monazite inclusions in apatite
719 porphyroblasts from the Hemlo gold deposit, Ontario, Canada. Mineralogical
720 Magazine, 57, 697-708.
721 Pan, Y., Fleet, M. E., and Macrae, N. D. (1993b) Late alteration in titanite (CaTiSiO5):
722 redistribution and remobilization of rare earth elements and implications for U/Pb and
723 Th/Pb geochronology and nuclear waste disposal. Geochimica et Cosmochimica Acta,
724 57, 355-367.
725 Pavlenko, A. S., Orlova, L. P., Akhmanova, M. V., and Tobelko, K. I. (1965) A thorium
726 fluorcarbonate–thorbastnäsite. Zapiski Vserossijskogo Mineralogiceskogo Obscestva,
727 94, 105-113.
728 Pecora, W. T., and Kerr, J. H. (1953) Burbankite and Calkinsite, 2 new Carbonate Minerals
729 from Montana. American Mineralogist, 38, 1169-1183.
730 Poitrasson, F., Oelkers, E., Schott, J., and Montel, J.-M. (2004) Experimental determination of
731 synthetic NdPO 4 monazite end-member solubility in water from 21 C to 300 C:
732 Implications for rare earth element mobility in crustal fluids. Geochimica et
733 Cosmochimica Acta, 68, 2207-2221.
734 Rankin, A. (2005) Carbonatite-associated rare metal deposits: composition and evolution of
735 ore-forming fluids–the fluid inclusion evidence. In R. Linnen & I. Samson, Eds., Rare
736 Metal Geochemistry and Ore Deposits, Geological Association of Canada, Short
737 Course Notes, p. 299-314.

738 Read, D., Andreoli, M. a. G., Knoper, M., Williams, C. T., and Jarvis, N. (2002) The
739 degradation of monazite: Implications for the mobility of rare-earth and actinide
740 elements during low-temperature alteration. European Journal of Mineralogy, 14, 487-
741 498.
742 Reischmann, T. (1995) Precise U/Pb age determination with baddeleyite (ZrO2), a case study
743 from the Phalaborwa igneous complex, South Africa. South African Journal of
744 Geology, 98, 1-4.
745 Sharygin, V. V., Zhitova, L. M., and Nigmatulina, E. N. (2011) Fairchildite K2Ca(CO3)2 in
746 phoscorites from Phalaborwa, South Africa: the first occurrence in alkaline carbonatite
747 complexes. Russian Geology and Geophysics, 52, 208-219.
748 Shunhua, H., Zonggang, W., Zhongnei, Z., and Songyu, H. (1986) An experimental study of
749 the conditions of the formation of bastnaesite. Acta Mineralogica Sinica, 6, 155-170.
750 Smith, M. P., Henderson, P., and Peishan, Z. (1999) Reaction relationships in the Bayan Obo
751 Fe-REE-Nb deposit Inner Mongolia, China: implications for the relative stability of
752 rare-earth element phosphates and fluorocarbonates. Contributions to Mineralogy and
753 Petrology, 134, 294-310.
754 Smith, M. P., Henderson, P., and Campbell, L. S. (2000) Fractionation of the REE during
755 hydrothermal processes: constraints from the Bayan Obo Fe-REE-Nb deposit, Inner
756 Mongolia, China. Geochimica et Cosmochimica Acta, 64, 3141-3160.
757 Solovova, I. P., Ryabchikov, I. D., Kogarko, L. N., and Konokova, N. N. (1998) Inclusions in
758 minerals of the Phalaborwa carbonatite complex. South Africa. Geochimija, 5, 435-
759 447.
760 Somina, M. Y. (1975) Dolomite and ankerite carbonatites from the East Siberia, 191 p. Nedra,
761 Moscow.

762 Stettler, E. H., De Beer, J. H., and Blom, M. P. (1989) Crustal domains in the northern
763 Kaapvaal Craton as defined by magnetic lineaments. Precambrian research, 45, 263-
764 276.
765 Tomašić, N., Gajović, A., Bermanec, V., Su, D. S., Linarić, M. R., Ntaflos, T., and Schlögl,
766 R. (2006) Recrystallization mechanisms of fergusonite from metamict mineral
767 precursors. Physics and Chemistry of Minerals, 33, 145-159.
768 Torró, L., Villanova, C., Castillo, M., Campeny, M., Gonçalves, A. O., and Melgarejo, J. C.
769 (2012) Niobium and rare earth minerals from the Virulundo carbonatite, Namibe,
770 Angola. Mineralogical Magazine, 76, 393-409.
771 Tropper, P., and Manning, C. E. (2005) Letter: Very low solubility of rutile in H2O at high
772 pressure and temperature, and its implications for Ti mobility in subduction zones.
773 American Mineralogist, 90, 502-505.
774 Uher, P., Ondrejka, M., Bačík, P., Broska, I., and Konečný, P. (2015) Britholite, monazite,
775 REE carbonates, and calcite: Products of hydrothermal alteration of allanite and
776 apatite in A-type granite from Stupné, Western Carpathians, Slovakia. Lithos, 236,
777 212-225.
778 Uken, R., and Watkeys, M. K. (1997) An interpretation of mafic dyke swarms and their
779 relationship with major mafic magmatic events on the Kaapvaal Craton and Limpopo
780 Belt. South African Journal of Geology, 100, 341-348.
781 Van Baalen, M. R. (1993) Titanium mobility in metamorphic systems: a review. Chemical
782 geology, 110, 233-249.
783 Verplanck, P. L., Mariano, A. N., and Mariano, A., Jr (2016) Rare Earth Element Ore
784 Geology of Carbonatites. In P. L. Verplanck & M. W. Hitzman, Eds., Rare Earth and
785 Critical Elements in Ore Deposits, p. 5-32. Reviews in Economic Geology, Society of
786 Economic Geologists, Littleton, CO.

787 Verwoerd, W. J. (1966) South African carbonatites and their probable mode of origin. Annals
788 of the University of Stellenbosch, 41(A2), 233 p. Stellenbosch University,
789 Stellenbosch.
790 Verwoerd, W. J., and Du Toit, M. C. (2006) The Phalaborwa and Schiel complexes. In M. R.
791 Johnson, C. R. Anhaeusser & R. J. Thomas, Eds., The Geology of South Africa, p.
792 291-299. Council for Geoscience, Pretoria.
793 Wall, F. (2014) Rare earth elements. In G. Gunn, Eds., Critical metals handbook, p. 312-339.
794 British Geological Survey, Nottingham, UK.
795 Wall, F., and Mariano, A. N. (1996) Rare earth minerals in carbonatites: a discussion centred
796 on the Kangankunde Carbonatite, Malawi. In A. P. Jones, F. Wall & C. T. Williams,
797 Eds., Rare Earth Minerals: Chemestry, Origin and Ore Deposits. Mineralogical
798 Society Series, p. 193-226. Chapman and Hall, London.
799 Wall, F., and Zaitsev, A. N. (2004a) Phoscorites and carbonatites from mantle to mine: the
800 key example of the Kola Alkaline Province, 503 p. The Mineralogical Society of Great
801 Britain and Ireland, London.
802 Wall, F., and Zaitsev, A. N. (2004b) Rare earth minerals in Kola carbonatites. In F. Wall & A.
803 N. Zaitsev, Eds., Phoscorites and carbonatites from mantle to mine: the key example
804 of the Kola Alkaline Province. , p. 341-373. Mineralogical Society Series,
805 Mineralogical Society, London, UK.
806 Wall, F., Le Bas, M. J., and Srivastava, R. K. (1993) Calcite and carbocernaite exsolution and
807 cotectic textures in a Sr, REE-rich carbonatite dyke from Rajasthan, India.
808 Mineralogical Magazine, 57, 495-495.
809 Wall, F., Zaitsev, A., Jones, A. P., and Mariano, A. N. (1997) Rare-earth rich carbonatites: a
810 review and latest results. Journal of the Czech Geological Society, 42, 49.
811 Wang, L., Yu, Y., Huang, X., Long, Z., and Cui, D. (2013) Toward greener comprehensive
812 utilization of bastnaesite: Simultaneous recovery of cerium, fluorine, and thorium

from bastnaesite leach liquor using HEH (EHP). Chemical Engineering Journal, 215, 162-167.

Williams-Jones, A. E., and Wood, S. A. (1992) A preliminary petrogenetic grid for REE fluorocarbonates and associated minerals. Geochimica et Cosmochimica Acta, 56, 725-738.

Wilson, M. G. C. (1998) Copper. In M. G. C. Wilson & C. R. Anhaeusser, Eds., The mineral resources of South Africa, p. 209-217. Council for Geoscience, Pretoria.

Wingate, M. T. D., and Compston, W. (2000) Crystal orientation effects during ion microprobe U–Pb analysis of baddeleyite. Chemical geology, 168, 75-97.

Wu, F.-Y., Yang, Y.-H., Li, Q.-L., Mitchell, R. H., Dawson, J. B., Brandl, G., and Yuhara, M. (2011) In situ determination of U–Pb ages and Sr–Nd–Hf isotopic constraints on the petrogenesis of the Phalaborwa carbonatite Complex, South Africa. Lithos, 127, 309-322.

Wyllie, P. J., Jones, A. P., and Deng, J. (1996) Rare earth elements in carbonate-rich melts from mantle to crust. In A. P. Jones, F. Wall & C. T. Williams, Eds., Rare Earth Minerals: Chemestry, Origin and Ore Deposits. Mineralogical Society Series, p. 77-103. Chapman and Hall, London.

Yaroshevskii, A. A., and Bagdasarov, Y. A. (2008) Geochemical Diversity of Minerals of the Pyrochlore Group. Geochemistry International, 46, 1245-1266.

Yuhara, M., Kohno, M., Kagami, H., Hiroi, Y., and Tsuchiya, N. (2003) Geochemistry of syenite of the Phalaborwa carbonatite complex, South Africa. Polar Geoscience, 16, 176-195.

Zaitsev, A. N., Wall, F., and Le Bas, M. J. (1998) REE-Sr-Ba minerals from the Khibina carbonatites, Kola Peninsula, Russia: their mineralogy, paragenesis and evolution. Mineralogical Magazine, 62, 225-250.

838 Zaitsev, A. N., Williams, C. T., Jeffries, T. E., Strekopytov, S., Moutte, J., Ivashchenkova, O.
839 V., Spratt, J., Petrov, S. V., Wall, F., Seltmann, R., and Borozdin, A. P. (2015) Reprint
840 of "Rare earth elements in phoscorites and carbonatites of the Devonian Kola Alkaline
841 Province, Russia: examples from Kovdor, Khibina, Vuoriyarvi and Turiy Mys
842 complexes". Ore Geology Reviews, 64, 477-498.
843 Zirner, A. L. K., Marks, M. a. W., Wenzel, T., Jacob, D. E., and Markl, G. (2015) Rare Earth
844 Elements in apatite as a monitor of magmatic and metasomatic processes: the
845 Ilímaussaq complex, South Greenland. Lithos, 228, 12-22.

846

847 ## LIST OF FIGURE CAPTIONS

848 **Figure 1.** Generalized geological map of the Palabora Complex (modified after Hanekom et
849 al. 1965; Fourie and De Jager 1986; Wilson 1998) and cross section of the Loolekop-
850 pipe in N-S direction showing the irregular ring structure of the pipe (modified and
851 extended after Wilson 1998).

852 **Figure 2.** Paragenetic scheme for carbonatites and phoscorite (blue field) of the Loolekop
853 deposit. Note: Main phases in bold, minor phases in plain style, accessory phases in
854 italics, REE phases in red.

855 **Figure 3.** General orthomagmatic mineral assemblages observed in carbonatites and
856 phoscorite from the Loolekop deposit. (a) euhedral apatite inclusion in partly
857 serpentinized forsterite. (b) Intergrowth of magmatic baddeleyite and thorianite. (c)
858 Euhedral inclusion of thorianite in apatite. (d) Calcite inclusion in apatite, which again
859 is enclosed in phlogopite. (E) Baddeleyite and apatite inclusions in phlogopite. (f)
860 Dolomite and phlogopite surrounded by ilmenite in magnetite. Baddeleyite included in
861 ilmenite. (g) Ilmenite with inclusions of phlogopite and magnetite, all included in

magnetite. (h) Spinel with baddeleyite and zirconolite included in magnetite. (i) Exsolved spinel cubes (note the equality of orientation) associated with exsolved ilmenite lamellae in magnetite. (j) Slightly rounded spinel with a rim of ilmenite in magnetite. (k) Ilmenite exsolution lamellae in magnetite. (l) Distinct dolomite accumulations partly enclosed in calcite with dolomite exsolution (arrow). (m) Sub-graphic intergrowth of vermicular dolomite exsolutions with calcite.

Figure 4. Textural appearances of fergusonite. (a) Rounded fergusonite partly included in magnetite. (b) Rounded fergusonite associated with zirconolite included in magnetite. And partly dissolved fergusonite with overgrown baddeleyite. Small baddelyite grain on the left side in contrast shows an overgrowth by fergusonite. (c) Rod-shaped REE-Ti-betafite partly included in magnetite. (d) Rod-shaped REE-Ti-betafites included in magnetite, calcite and dolomite.

Figure 5. Textural appearances of REE-F-carbonates. (a) Partly dissolved REEFC-I needle. (b) REEFC-I partly included in chalcopyrite. Note the strong dissolved parts of REEFC-I outside the sulphide enclosure. (c) & (d) Partly dissolved REEFC-I with interdigitating parisite/synchysite and bastnäsite, and (d) the additional presence of strontianite and fluorite. (e) & (f) Relics of monazite around apatite with interlocked REEFC-II a. Monazite decomposed to secondary REEFC-II a needles and secondary apatite (ap-II). (g) Carbonate vein through calcite with exsolved dolomite and REEFC-II b. The enlargement shows the intergrowth with magnetite. Note the tiny secondary thorianite inclusions in magnetite and REEFC-II b. (h) REEFC-II b intergrown with magnetite and anzaite with inclusions of secondary “fusiform” thorite. Recrystallized zone is located next to a serpentinized area.

Figure 6. Textural appearances of monazite and britholite. (a) Tumor-like expansions of monazite rim around apatite. (b) Tiny relics of apatite enclosed by calcite with a thick

887 rim and irregular precipitation of monazite. (c) Monazite partly enclosed by sulphides
888 with apatite rim where sulphide shows valleriitization. Note the lack of apatite rim at
889 monazite where no valleriitization took place. (d) Strongly altered monazite with
890 formation of secondary apatite associated with valleriitization of sulphides. Note thorite
891 inclusions in valleriite. (e) Monazite and britholite in equilibrium around serpentinized
892 forsterite and apatite. The red dashed line marks the border between britholite and
893 monazite. (f) Thick britholite rim around serpentinized forsterite. (g) Britholite around
894 forsterite replaced by chondrodite and serpentine. (h) Britholite associated with
895 phlogopite and chlorite.

896 **Figure 7.** Textural appearances of ancylite and cordylite. (a) Heterogeneous ancylite needle
897 with light parts reflecting intergrown baryte, darkest parts reflecting high Ca, low Sr
898 and low REE contents and medium light parts reflecting high Sr and low Ca content
899 with high concentration of REE. (b) rod-like/partly irregular ancylite with an inclusion
900 of baryte. (c) (c) Ancylite associated with cordylite. (d) Ancylite intergrowth with
901 magnetite in recrystallized carbonate vein. Dark rims around dolomite represent
902 serpentine. (e) Ancylite, pseudomorph after completely dissolved primary thorianite,
903 with thorite inclusion enclosed in ancylite, serpentine and magnetite, all associated
904 with recrystallized calcite. (f) Cracks in apatite filled with ancylite, celestine and
905 magnetite**.** (g) Cordylite with thin tail filling a crack in calcite. (h) Patchy zonation of
906 cordylite shows the heterogeneity of this phase.

907 **Figure 8.** Textural appearances of anzaite. (a) Compositionally zoned anzaite completely
908 replacing ilmenite at magnetite. Anzaite shows mostly patchy zoning with the brightest
909 areas having high REE/Ti ratios and darker areas showing the opposite. (b) Anzaite
910 replacing ilmenite with ilmenite relics enclosed by anzaite. (c) Dissolved ilmenite
911 lamellae (partly filled with calcite) with relictic ilmenite in the center of the lamellae

and precipitation of anzaite at a shortage within the former lamellae. The upper part of the image displays the same phenomenon with a batch of ilmenite partly dissolved and filled by calcite and showing marginal precipitation of anzaite. (d) Partly replacement of ilmenite by anzaite as well as precipitation of anzaite around ilmenite relicts. (e) Anzaite associated with valleriite replacing chalcopyrite. (f) Association of anzaite, valleriite, serpentine and secondary apatite (ap-III). Note the intergrowth of valleriite, ap-III and anzaite.

Figure 9. Scheme of REE mineral precipitation during different evolutionary stages of the Palabora carbonatites. Estimated temperatures after (Fernandez et al. 1977; Solovova et al. 1998; Fleet 2006; Sharygin et al. 2011; Chakhmouradian et al. 2015). Roman numbers (I-III) refer to diagrams in Fig. 13.

Figure 10. Qualitative activity diagrams illustrating the relative stabilities of different REE mineral phases. Numbers in brackets refer to reactions mentioned in the text. Note the necessity of REE introduction for the formation of monazite and britholite during stage 2 (I & II) as well as the locally controlled variability of F in stage 2 and 4 fluids (II & III). The activity of "Ca^{2+}" in diagram III reflects the combination of the alkali- and alkaline earth metals Ca^{2+}+Sr^{2+}+Ba^{2+}+Na^{+} for simplification.

This is a preprint, the final version is subject to change, of the American Mineralogist (MSA)
Cite as Authors (Year) Title. American Mineralogist, in press.
(DOI will not work until issue is live.) DOI: http://dx.doi.org/10.2138/am-2017-6004

Table 1. Chemical formulae of the minerals mentioned in the text and figures

Mineral	Abbr.	Formula	Mineral
SILICATES:			**CARBONATES:**
chlorite	chl	$(Mg_4Al_2)Si_3Al)O_{10}(OH)_8$	ancylite-(Ce)
chondrodite	chn	$(Mg,Fe)_5(SiO_4)_2(F,OH)2$	bastnäsite-(Ce)
fluorbritholite-(Ce)	bri	$Ca_2(REE)_3(SiO_4)_3(F,OH)$	burbankite
olivine	ol	$(Mg,Fe)SiO_4$	calcite
phlogopite	phl	$KMg_3(Si_3Al)O_{10}(OH,F)_2$	carbocernaite
serpentine	srp	$Mg_6Si_4O_{10}(OH)_8$	cordylite-(Ce)
thorite	thr	$ThSiO_4$	dolomite
			parisite-(Ce)
OXIDES:			strontianite
anzaite-(Ce)	anz	$(REE)_4FeTi_6O_{18}(OH,F)_2$	synchysite-(Ce)
baddeleyite	bdl	ZrO_2	barytocalcite
REE-Ti-betafite-(Ce)	btf	$(REE,Ca)_2Ti_2O_6(O,OH,F)$	
fergusonite-(Nd)-β	frg	$(REE)NbO_4$	**SULPHATES:**
ilmenite	ilm	$FeTiO_3$	baryte
magnetite	mgt	Fe_3O_4	celestine
spinel	spl	$MgAl_2O_4$	
thorianite	thn	ThO_2	**PHOSPHATES:**
zirconolite	zrc	$CaZrTi_2O_7$	fluorapatite
			monazite-(Ce)
SULPHIDES:			
bornite	bn	Cu_5FeS_4	**HALIDES:**
chalcopyrite	cp	$CuFeS_2$	fluorite
galena	gn	PbS	
valleriite	val	$2((Fe,Cu)S)•1.53((Mg,Al)(OH)_2)$	

Abbr.	Formula
anc	$(Sr,Ca)(REE)(CO_3)_2(OH)\bullet H_2O$
bsn	$(REE,Ca)(CO_3)_2F$
bur	$(Ca,Na)_3(Sr,REE,Ba)_3(CO_3)_5$
cal	$CaCO_3$
cbc	$(Ca,Na)(Sr,REE,Ba)(CO_3)_2$
cdy	$(Ca,Na)Ba(REE)_2(CO_3)_3F_2$
dol	$CaMg(CO_3)_2$
pst	$Ca(REE)_2(CO_3)_3F_2$
str	$(Sr,Ca,Ba)CO_3$
syn	$Ca(REE)(CO_3)_2F$
bcl	$BaCa(CO_3)_2$
brt	$BaSO_4$
cls	$SrSO_4$
ap	$Ca_5(PO_4)_3(F,OH)$
mnz	$(REE,Ca)PO_4$
fl	CaF_2

This is a preprint, the final version is subject to change, of the American Mineralogist (MSA)
Cite as Authors (Year) Title. American Mineralogist, in press.
(DOI will not work until issue is live.) DOI: http://dx.doi.org/10.2138/am-2017-6004

Table 2. Mean electron microprobe analyses of REE minerals

in wt%	**fergusonite**		**REE-Ti-btf**		**monazite**		**britholite**		**cord**
	avg.	st.dev.	avg.	st.dev.	avg.	st.dev.	avg.	st.dev.	avg.
La_2O_3	4.18	0.52	10.12	0.74	18.92	3.39	8.43	0.90	10.03
Ce_2O_3	17.50	0.60	29.15	0.65	33.90	0.62	28.39	0.76	19.39
Pr_2O_3	4.68	0.37	4.67	0.16	3.85	0.67	4.65	0.46	3.82
Nd_2O_3	18.63	0.85	15.09	0.70	9.88	2.20	17.80	0.84	7.78
Sm_2O_3	3.64	0.70	2.30	0.16	0.30	0.27	2.82	0.33	0.33
Eu_2O_3	1.33	0.84	0.68	0.05	0.39	0.13	0.57	0.16	-
Gd_2O_3	2.19	0.57	1.56	0.13	1.03	0.93	2.61	0.40	0.29
Y_2O_3	1.53	0.23	1.90	0.36	0.94	0.14	-		0.31
$\sum REE_2O_3+Y_2O_3$	*53.68*		*65.47*		*69.21*		*65.27*		*41.95*
ThO_2	0.75	0.83	-		0.04	0.06	-		-
UO_2	-		-		0.04	0.04	0.04	0.03	-
PbO	-		-		0.03	0.03	-		-
TiO_2	0.13	0.58	32.69	0.61	-		-		-
Nb_2O_5	42.76	0.29	0.07	0.12	-		-		-
Ta_2O_5	-		-		-		-		-
SnO_2	-		-		-		-		-
FeO	0.58	0.54	0.03	0.65	-		0.09	0.09	-
Al_2O_3	-		-		-		0.01	0.02	-
MgO	-		-		-		0.02	0.08	-
Na_2O	-		-		-		-		1.49
CaO	0.58	0.53	0.36	0.86	0.32	0.41	11.12	0.41	3.03
SrO	-		-		-		-		4.43
BaO	-		-		-		-		22.05
SiO_2	-		-		0.21	0.06	19.88	0.29	-
P_2O_5	-		-		29.6	0.42	1.9	0.39	-
CO_2*	-		-		-		-		25.53
F	0.48	0.1	0.79	0.05	-		2.26	0.28	2.59
$-O=F_2$	0.20		0.33				0.95		1.09
TOTAL	98.76		99.08		99.45		99.64		99.98
H_2O*	-		-		-		-		-
	n=11		n=18		n=75		n=52		n=

Notes: below detection limit (-), standard deviation 1 sigma (st.dev.), CO_2* and H_2O* calculated by stoichi

This is a preprint, the final version is subject to change, of the American Mineralogist (MSA)
Cite as Authors (Year) Title. American Mineralogist, in press.
(DOI will not work until issue is live.) DOI: http://dx.doi.org/10.2138/am-2017-6004

ylite	**ANC-I**		**ANC-II**		**Bsn-I**		**Bsn-II**		**synch**
st.dev.	avg.	st.dev.	avg.	st.dev.	avg.	st.dev.	avg.	st.dev.	avg.
0.27	16.23	0.84	11.51	1.30	17.27	0.91	23.86	0.79	16.34
0.35	24.23	0.67	24.45	0.38	34.13	0.77	33.29	0.80	21.81
0.62	4.74	0.34	4.77	0.26	5.13	0.55	4.34	0.78	2.87
0.25	5.89	0.17	9.98	0.29	14.78	0.89	10.46	0.58	9.48
0.27	0.44	0.37	0.52	0.19	1.38	0.72	0.54	0.27	0.58
	-		-		-		-		-
0.21	-		-		0.78	0.19	0.24	0.21	0.08
0.22	-		-		-		-		0.05
	51.53		*51.23*		*73.47*		*72.73*		*51.21*
	0.01	0.07	0.63	0.07	0.07	0.08	0.36	0.51	-
	-		-		-		-		-
	-		-		-		-		-
	-		-		-		-		-
	-		-		-		-		-
	-		-		-		-		-
	-		-		-		-		-
	-		-		-		-		-
	-		-		-		-		-
	-		-		-		-		-
0.68	0.05	0.01	-		0.03	0.02	-		-
0.22	2.17	0.94	1.12	0.22	0.13	0.12	1.44	0.42	17.37
0.55	17.32	0.54	18.36	0.32	0.39	0.4	-		-
0.84	0.26	0.21	0.06	0.06	0.05	0.26	-		-
	-		-		-		-		-
	-		-		-		-		-
	23		22.5		20.92		20.64		27.47
0.14	0.22	0.14	0.38	0.14	8.53	0.77	8.35	0.81	6.01
	0.09		0.16		3.58		3.51		2.52
	94.47		94.12		100.01		100.01		99.54
	4.60	0.91	4.42	0.89	-		-		-
11	n=10		n=12		n=67		n=52		n=
ɔmetry									

This is a preprint, the final version is subject to change, of the American Mineralogist (MSA)
Cite as Authors (Year) Title. American Mineralogist, in press.
(DOI will not work until issue is live.) DOI: http://dx.doi.org/10.2138/am-2017-6004

ıysite	parisite		anzaite	
st.dev.	avg.	st.dev.	avg.	st.dev.
0.89	17.54	0.59	4.54	0.34
0.96	28.92	0.88	24.86	0.46
0.46	3.76	0.60	4.34	0.22
0.87	9.77	0.91	13.20	0.42
0.24	0.85	0.29	1.14	0.12
	-		1.61	0.12
0.09	0.39	0.15	0.92	0.28
0.07	0.27	0.10	1.41	0.14
	61.50		*52.02*	
	0.06	0.04	-	
	-		-	
	-		-	
	-		38.41	0.37
	-		0.03	0.11
	-		-	
	-		-	
	-		6.9	0.28
	-		0.01	0.03
	-		-	
	-		-	
0.82	9.81	0.92	0.29	0.03
	-		-	
	-		-	
	-		-	
	-		-	
	24.28		-	
0.76	7.12	0.79	0.54	0.18
	2.99		0.23	
	99.78		97.97	
	-		1.22	0.21
=7	n=11		n=15	

Table 2. (continued)

	fergusonite	**REE-Ti-btf**	**monazite**	**britholite**	**cord**
in apfu	4(O)	6.82(O)	4(O)	12(O)	4(C
La	0.08	0.30	0.28	0.44	0.
Ce	0.32	0.87	0.49	1.45	0.
Pr	0.09	0.14	0.06	0.24	0.
Nd	0.34	0.44	0.14	0.89	0.
Sm	0.06	0.07	-	0.14	0.
Eu	0.02	0.02	0.01	0.06	-
Gd	0.04	0.04	0.01	0.12	0.
Y	0.04	0.08	0.02	-	0.
∑REE+Y	0.99	1.96	1.01	3.34	1.
Th	0.01	-	-	-	-
U	-	-	-	-	-
Pb	-	-	-	-	-
TiO	-	2.00	-	-	-
Nb	0.98	0.01	-	-	-
Ta	-	-	-	-	-
Sn	-	-	-	-	-
Fe	0.02	0.002	-	0.01	-
Al	-	-	-	-	-
Mg	-	-	-	-	-
Na	-	-	-	-	0.
Ca	-	0.03	0.01	1.67	0.
Sr	-	-	-	-	0.
Ba	-	-	-	-	0.
Si	-	-	0.01	2.79	-
P	-	-	0.99	0.23	-
∑Cation	2.00	4.00	2.02	8.04	3.
F	0.08	0.18	-	0.99	0.
OH					
H_2O					

This is a preprint, the final version is subject to change, of the American Mineralogist (MSA)
Cite as Authors (Year) Title. American Mineralogist, in press.
(DOI will not work until issue is live.) DOI: http://dx.doi.org/10.2138/am-2017-6004

ylite	ANC-I	ANC-II	Bsn-I	Bsn-II	synch
	Structural formulae calculated for				
$O_3)^{2-}$	$2(CO_3)^{2-}$	$2(CO_3)^{2-}$	$1(CO_3)^{2-}$	$1(CO_3)^{2-}$	$2(C($
43	0.38	0.28	0.23	0.31	0.3
82	0.56	0.58	0.45	0.43	0.4
15	0.11	0.11	0.07	0.06	0.(
32	0.13	0.23	0.19	0.13	0.2
01	0.01	0.01	0.02	0.01	0.(
-	-	-	-	-	-
01	-	-	0.01	-	-
02	-	-	-	-	-
76	1.19	1.21	0.97	0.94	0.9
-	-	0.01	-	-	-
-	-	-	-	-	-
-	-	-	-	-	-
-	-	-	-	-	-
-	-	-	-	-	-
-	-	-	-	-	-
-	-	-	-	-	-
-	-	-	-	-	-
-	-	-	-	-	-
-	-	-	-	-	-
33	0.01	-	-	-	-
37	0.15	0.08	-	0.05	0.9
30	0.63	0.69	0.01	-	-
99	0.01	-	-	-	-
-	-	-	-	-	-
-	-	-	-	-	-
75	1.99	1.99	0.98	0.99	1.9
94	0.04	0.08	0.96	0.94	1.(
	1.15	1.13			
	0.81	0.79			

This is a preprint, the final version is subject to change, of the American Mineralogist (MSA)
Cite as Authors (Year) Title. American Mineralogist, in press.
(DOI will not work until issue is live.) DOI: http://dx.doi.org/10.2138/am-2017-6004

ıysite	parisite	anzaite
$O_3)^{2-}$	$3(CO_3)^{2-}$	19.66(O)
32	0.59	0.34
43	0.96	1.85
06	0.12	0.32
17	0.32	0.96
01	0.03	0.08
-	-	0.11
-	0.01	0.06
-	0.01	0.15
99	2.04	3.87
-	-	-
-	-	-
-	-	-
-	-	5.88
-	-	0.002
-	-	-
-	-	-
-	-	1.17
-	-	0.002
-	-	-
-	-	-
99	0.95	0.06
-	-	-
-	-	-
-	-	-
-	-	-
98	2.99	10.98
02	2.03	0.34
		1.66

This is a preprint, the final version is subject to change, of the American Mineralogist (MSA)
Cite as Authors (Year) Title. American Mineralogist, in press.
(DOI will not work until issue is live.) DOI: http://dx.doi.org/10.2138/am-2017-6004

Fig. 1

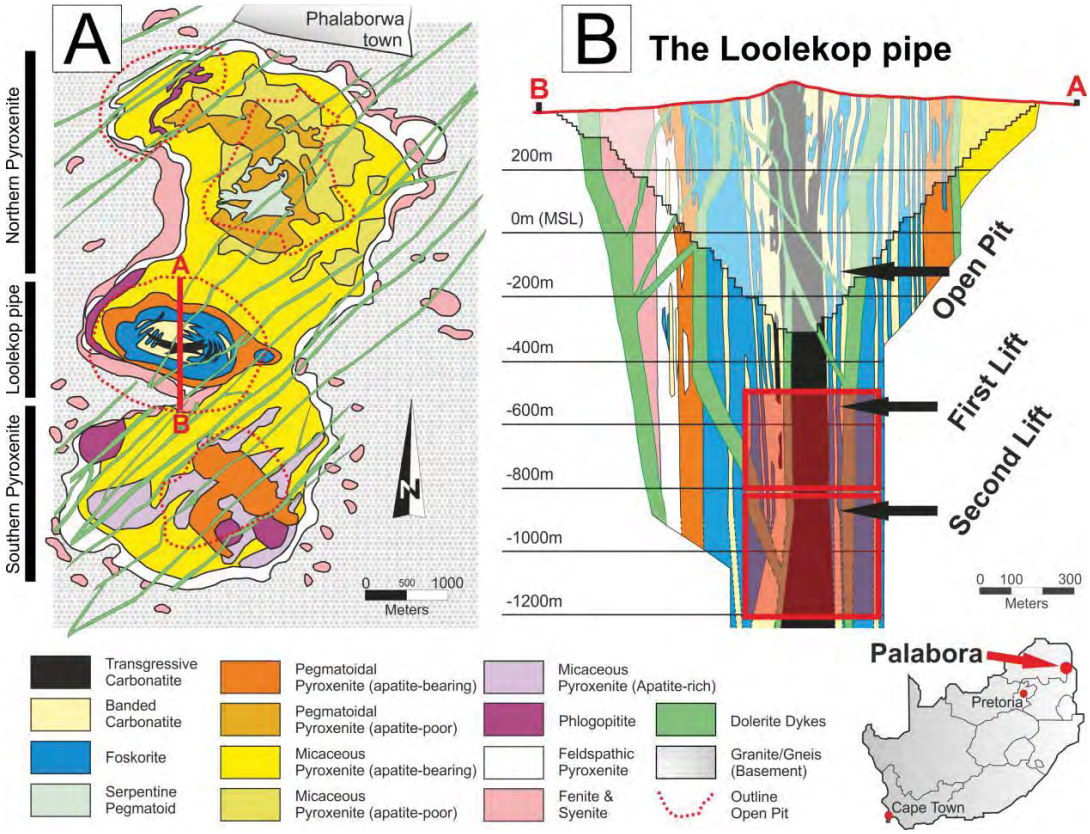

This is a preprint, the final version is subject to change, of the American Mineralogist (MSA)
Cite as Authors (Year) Title. American Mineralogist, in press.
(DOI will not work until issue is live.) DOI: http://dx.doi.org/10.2138/am-2017-6004

Fig. 2

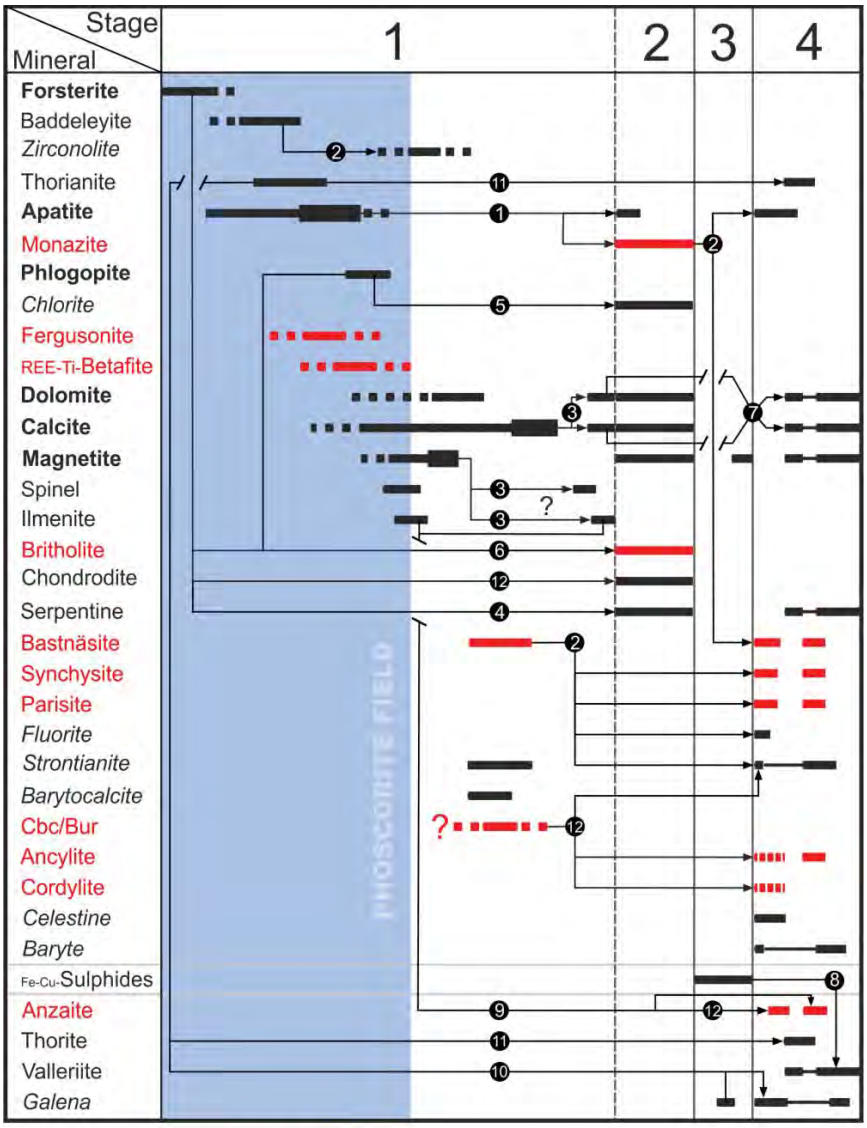

Stage of mineral formation:
(**1**) Ortho-Magmatic Stage (**2**) Late-Magmatic Stage
(**3**) Sulphide Stage (**4**) Post-Magmatic Stage

❶ Redistribution of P ❷ Alteration ❸ Exsolution ❹ Serpentinization
❺ Chloritization ❻ Redistribution of Si ❼ Recrystallization
❽ Valleriitization ❾ Redistribution of Ti ❿ Redistribution of Pb
⓫ Redistribution of Th ⓬ Replacement

This is a preprint, the final version is subject to change, of the American Mineralogist (MSA)
Cite as Authors (Year) Title. American Mineralogist, in press.
(DOI will not work until issue is live.) DOI: http://dx.doi.org/10.2138/am-2017-6004

Fig. 3

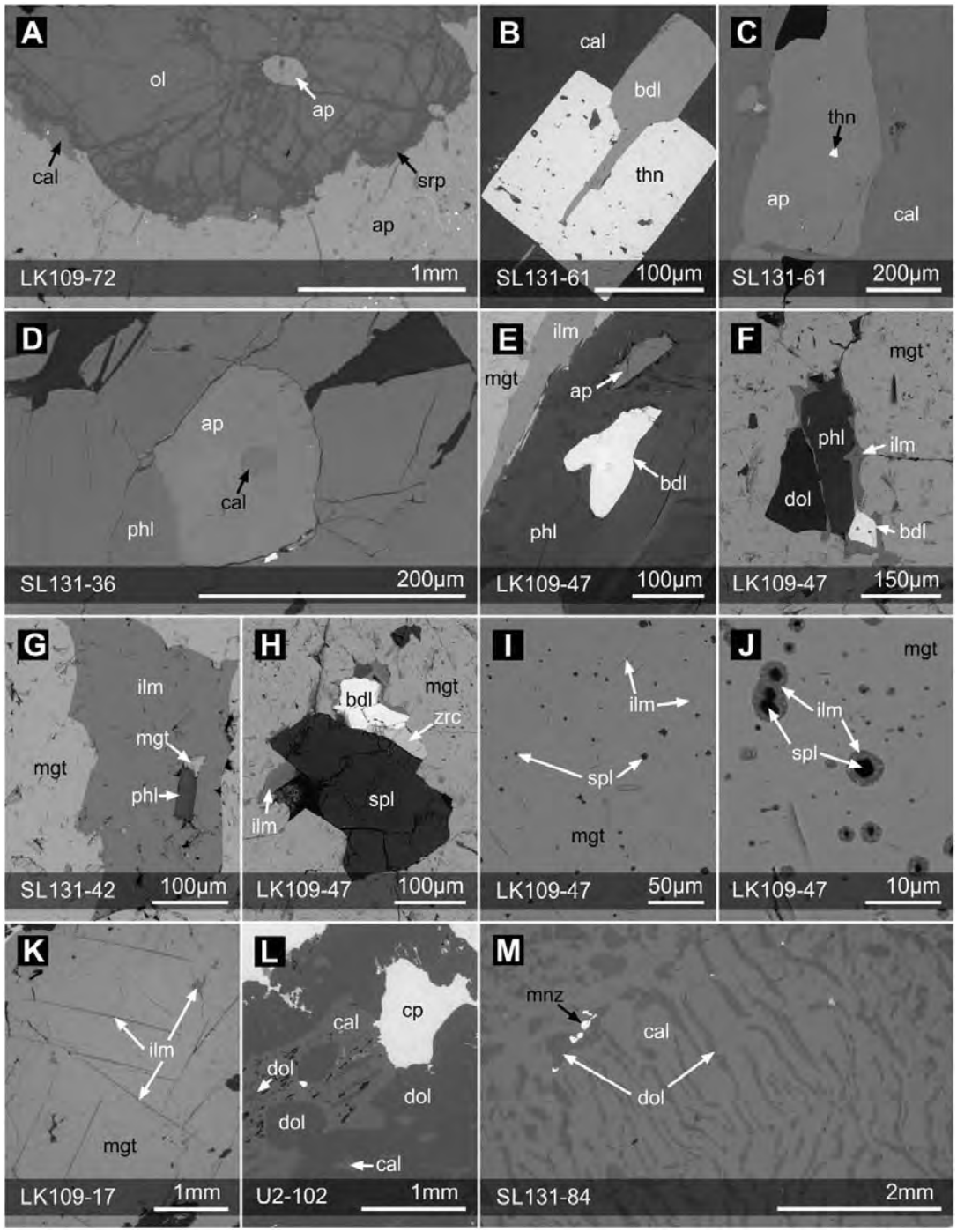

This is a preprint, the final version is subject to change, of the American Mineralogist (MSA)
Cite as Authors (Year) Title. American Mineralogist, in press.
(DOI will not work until issue is live.) DOI: http://dx.doi.org/10.2138/am-2017-6004

Fig. 4

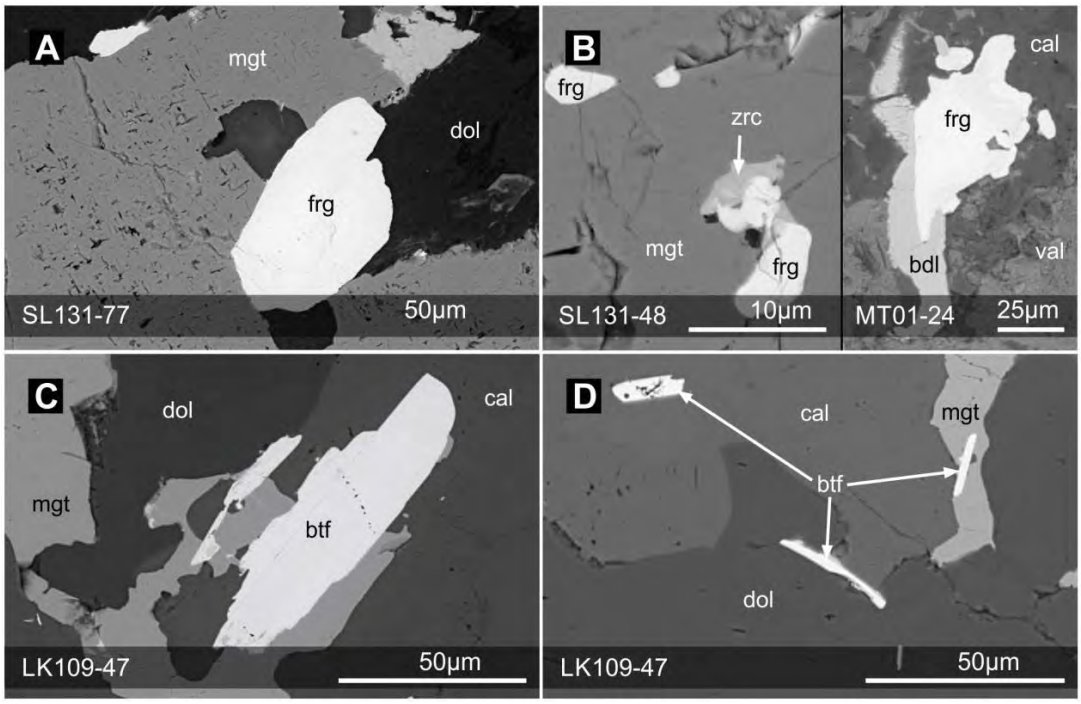

This is a preprint, the final version is subject to change, of the American Mineralogist (MSA)
Cite as Authors (Year) Title. American Mineralogist, in press.
(DOI will not work until issue is live.) DOI: http://dx.doi.org/10.2138/am-2017-6004

Fig. 5

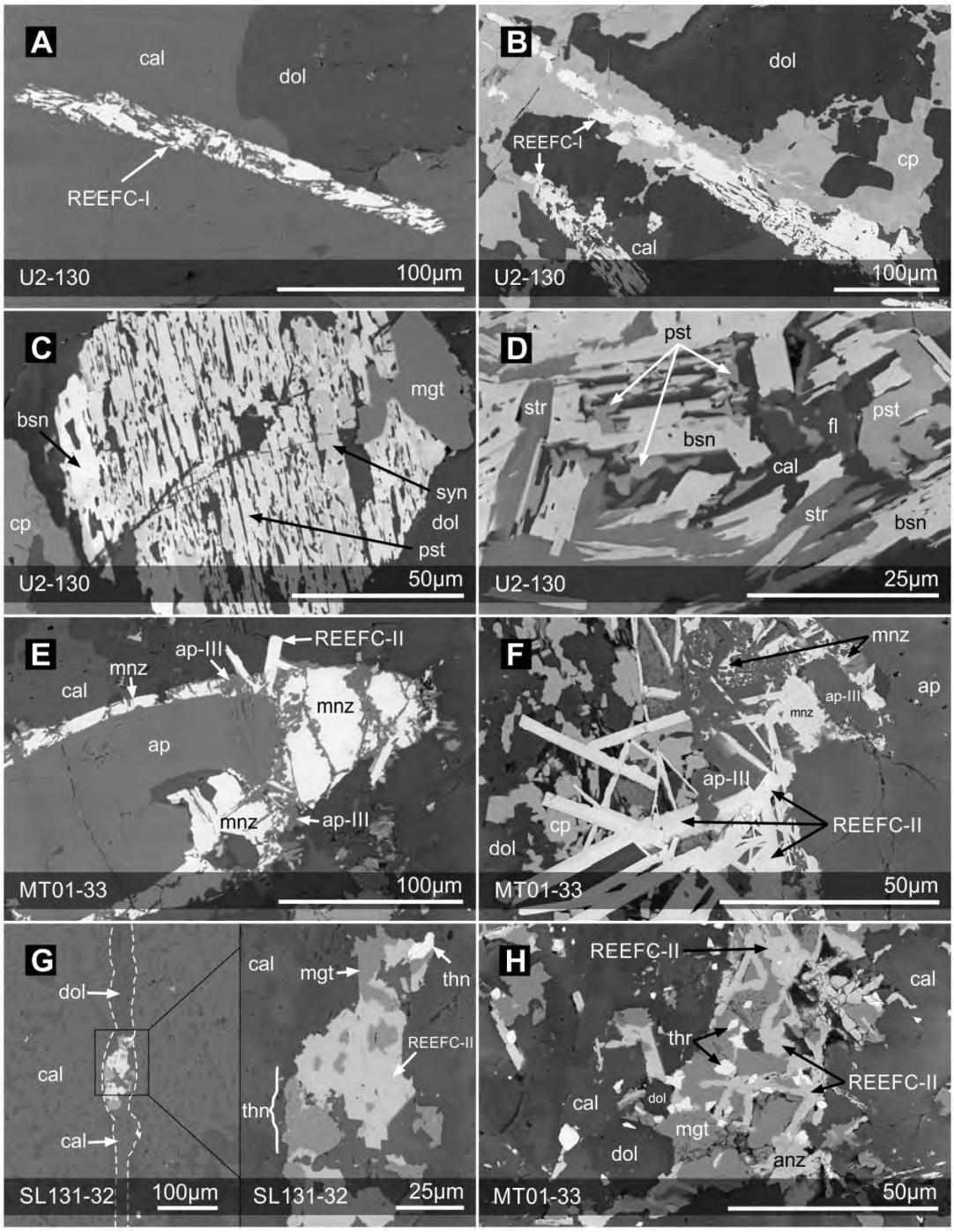

This is a preprint, the final version is subject to change, of the American Mineralogist (MSA)
Cite as Authors (Year) Title. American Mineralogist, in press.
(DOI will not work until issue is live.) DOI: http://dx.doi.org/10.2138/am-2017-6004

Fig. 6

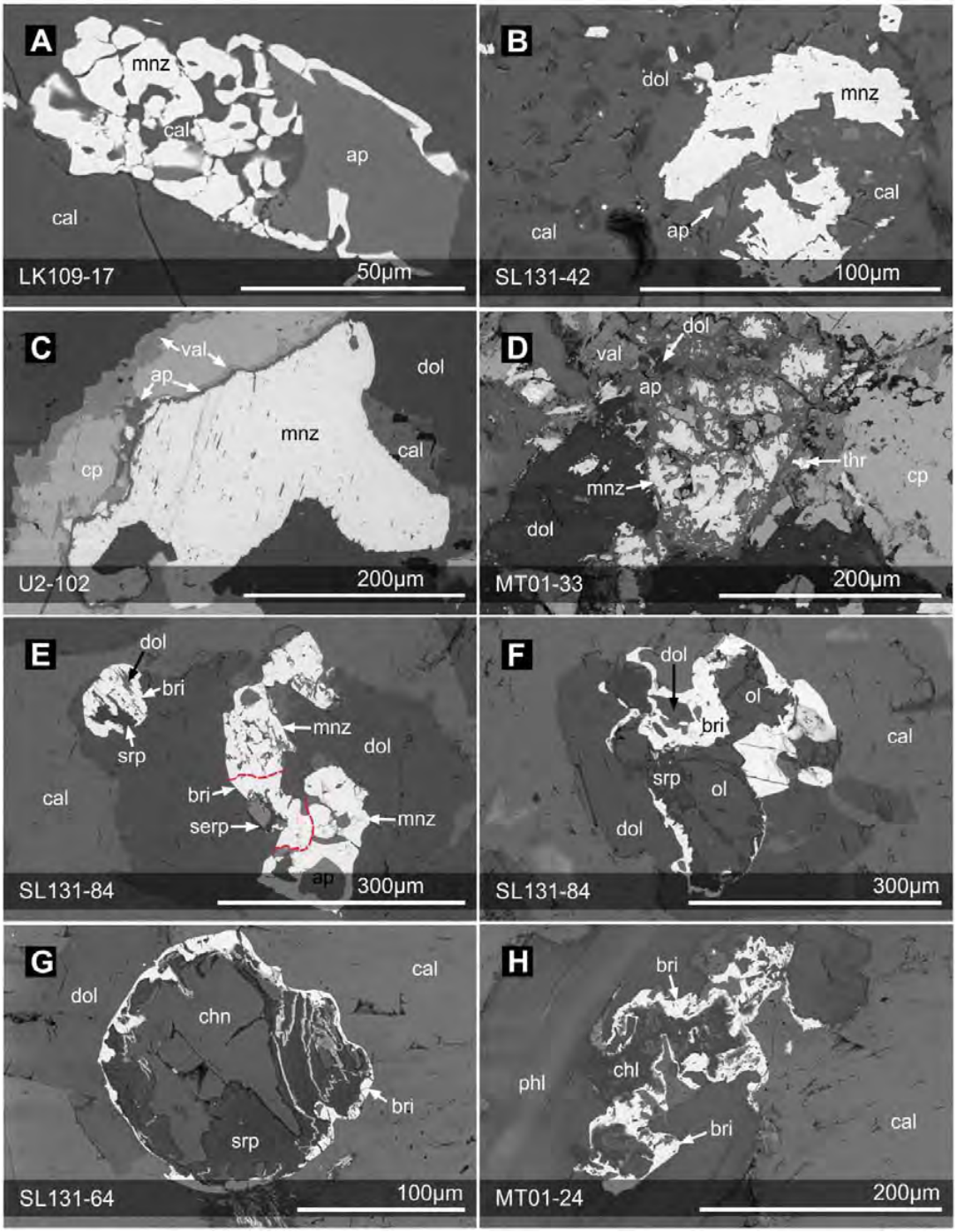

This is a preprint, the final version is subject to change, of the American Mineralogist (MSA)
Cite as Authors (Year) Title. American Mineralogist, in press.
(DOI will not work until issue is live.) DOI: http://dx.doi.org/10.2138/am-2017-6004

Fig. 7

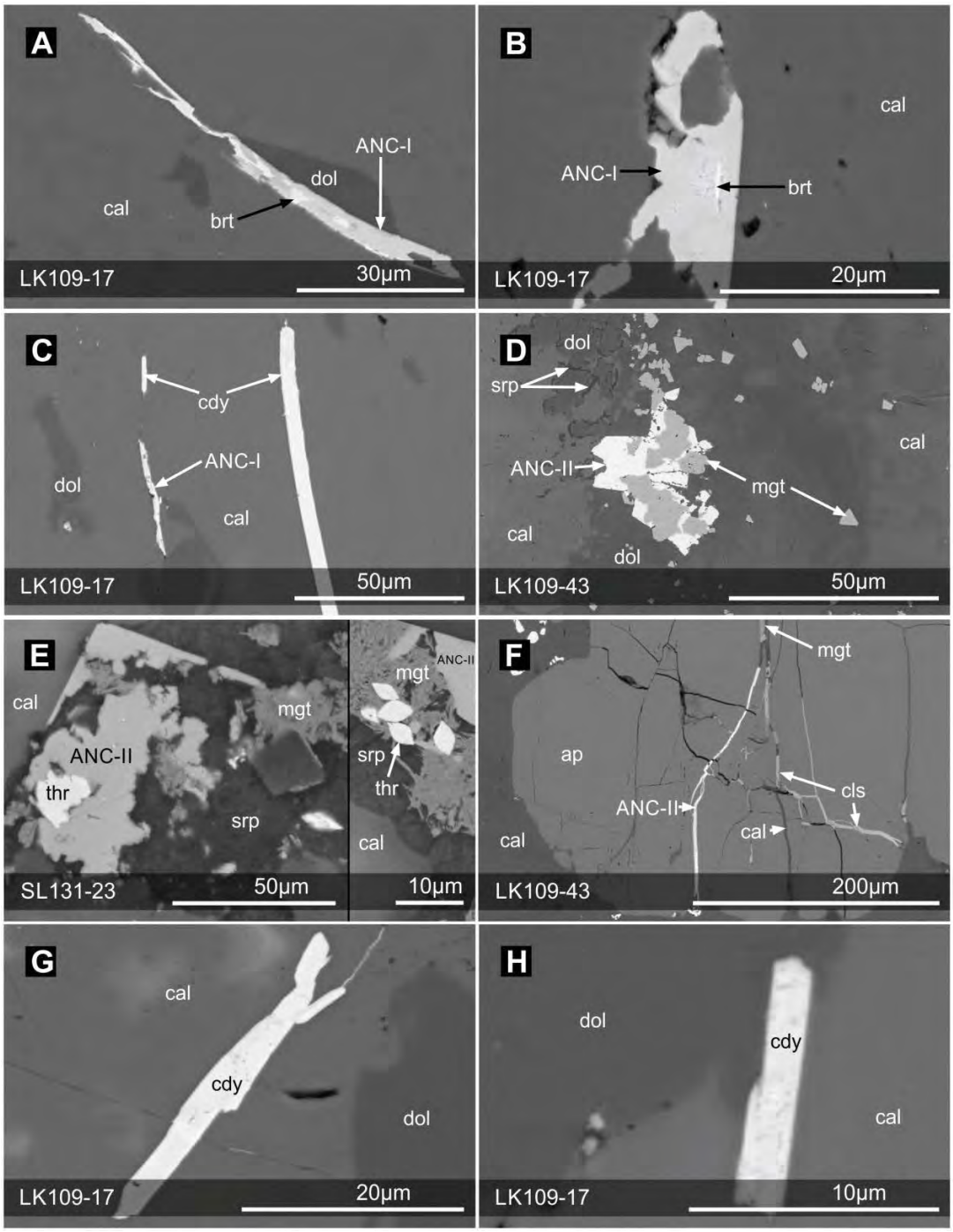

This is a preprint, the final version is subject to change, of the American Mineralogist (MSA)
Cite as Authors (Year) Title. American Mineralogist, in press.
(DOI will not work until issue is live.) DOI: http://dx.doi.org/10.2138/am-2017-6004

Fig. 8

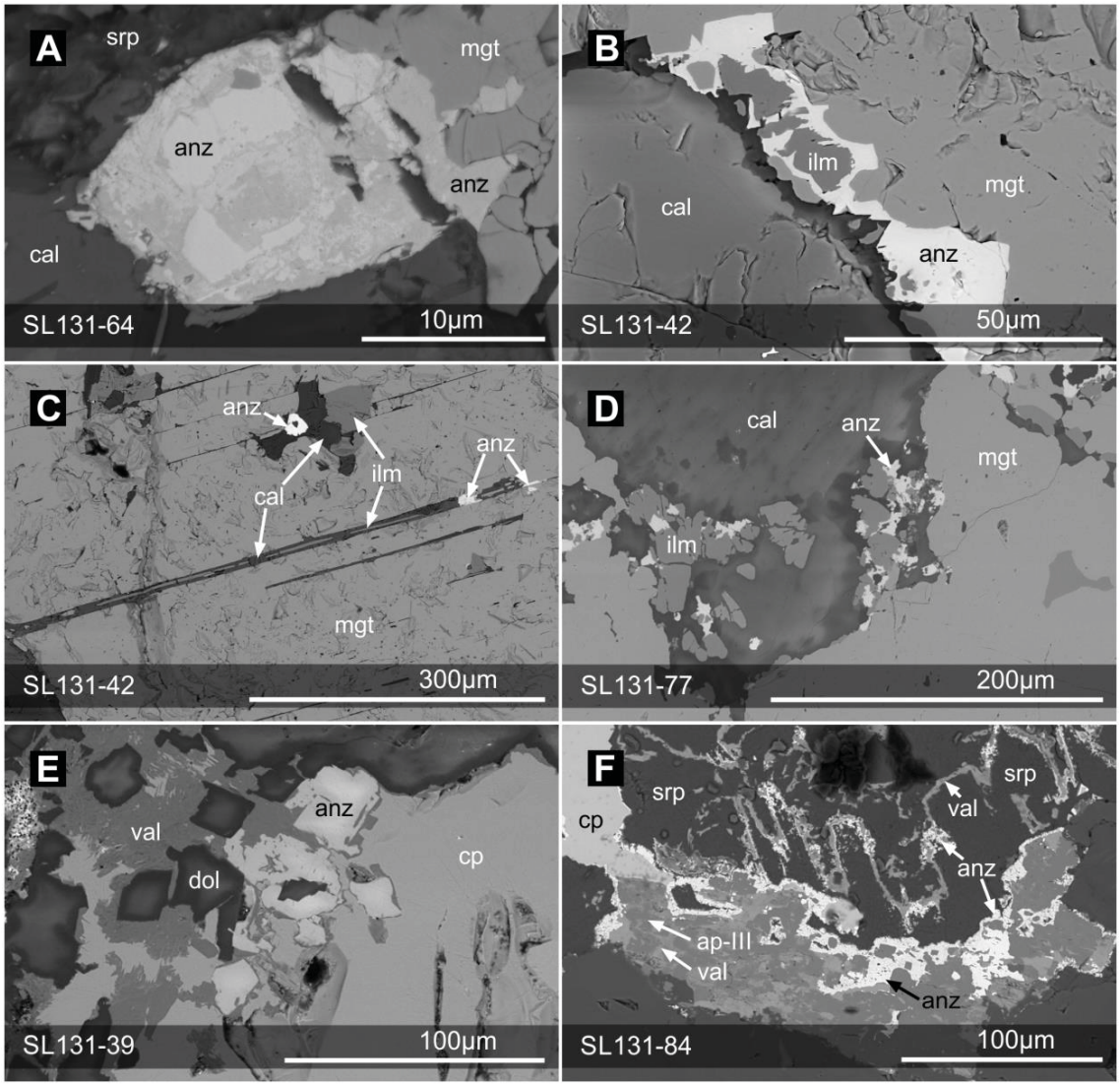

This is a preprint, the final version is subject to change, of the American Mineralogist (MSA)
Cite as Authors (Year) Title. American Mineralogist, in press.
(DOI will not work until issue is live.) DOI: http://dx.doi.org/10.2138/am-2017-6004

Fig. 9

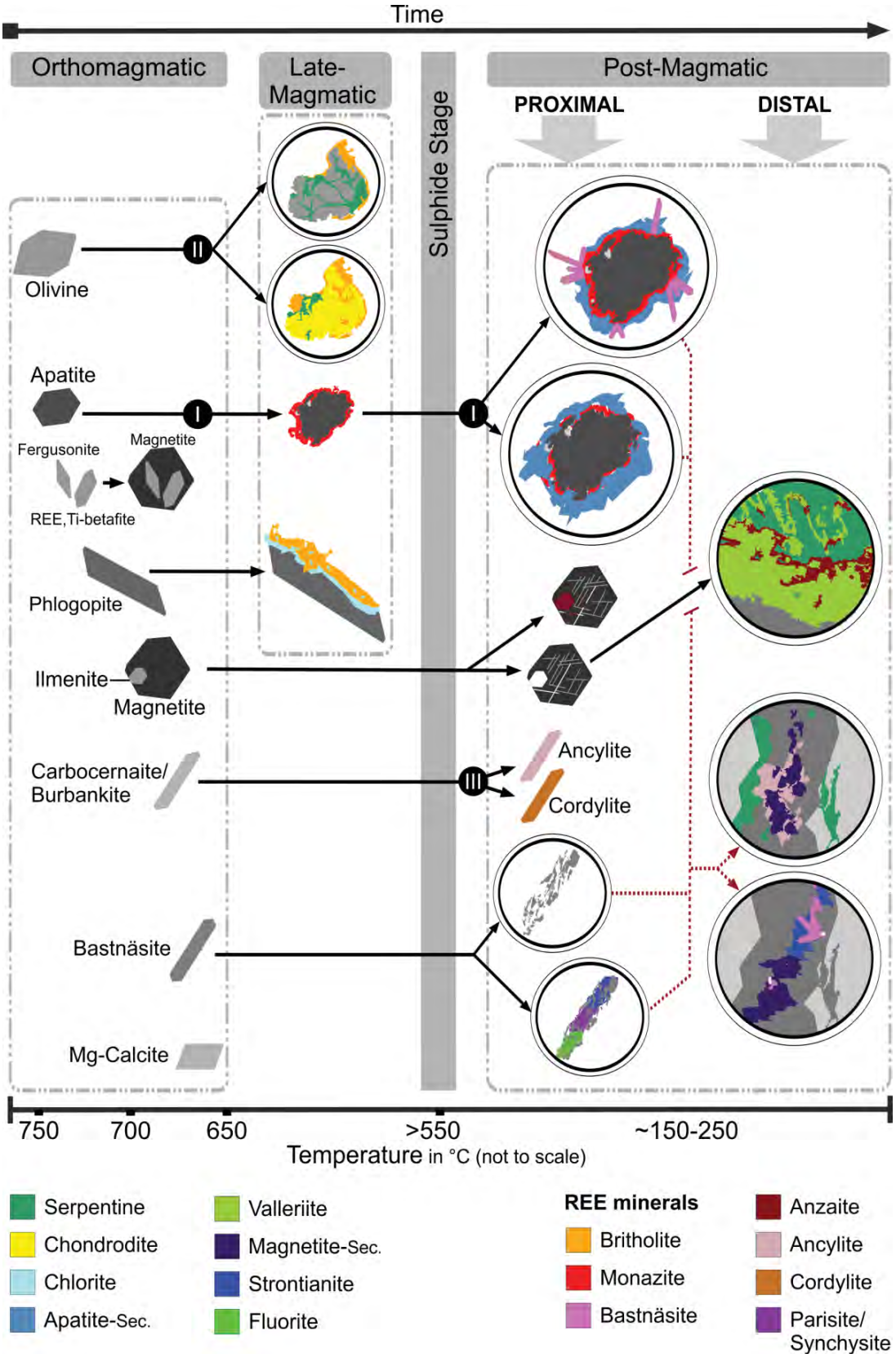

This is a preprint, the final version is subject to change, of the American Mineralogist (MSA)
Cite as Authors (Year) Title. American Mineralogist, in press.
(DOI will not work until issue is live.) DOI: http://dx.doi.org/10.2138/am-2017-6004

Fig. 10